UC Irvine
UC Irvine Previously Published Works

Title
Aerosols from biomass burning over the tropical South Atlantic region: Distributions and impacts

Permalink
https://escholarship.org/uc/item/8j37z8xk

Journal
Journal of Geophysical Research, 101(D19)

ISSN
0148-0227

Authors
Anderson, Bruce E
Grant, William B
Gregory, Gerald L
et al.

Publication Date
1996-10-30

DOI
10.1029/96jd00717

Copyright Information
This work is made available under the terms of a Creative Commons Attribution License, availalbe at https://creativecommons.org/licenses/by/4.0/

Peer reviewed

eScholarship.org Powered by the California Digital Library
University of California

JOURNAL OF GEOPHYSICAL RESEARCH, VOL. 101, NO. D19, PAGES 24,117–24,137, OCTOBER 30, 1996

Aerosols from biomass burning over the tropical South Atlantic region: Distributions and impacts

Bruce E. Anderson,[1] William B. Grant,[1] Gerald L. Gregory,[1] Edward V. Browell,[1] James E. Collins Jr.,[2] Glen W. Sachse,[3] Donald R. Bagwell,[4] Charles H. Hudgins,[4] Donald R. Blake,[5] and Nicola J. Blake[5]

Abstract. The NASA Global Tropospheric Experiment (GTE) Transport and Atmospheric Chemistry Near the Equator—Atlantic (TRACE A) expedition was conducted September 21 through October 26, 1992, to investigate factors responsible for creating the seasonal South Atlantic tropospheric ozone maximum. During these flights, fine aerosol (0.1–3.0 μm) number densities were observed to be enhanced roughly tenfold over remote regions of the tropical South Atlantic and greater over adjacent continental areas, relative to northern hemisphere observations and to measurements recorded in the same area during the wet season. Chemical and meteorological analyses as well as visual observations indicate that the primary source of these enhancements was biomass burning occurring within grassland regions of north central Brazil and southeastern Africa. These fires exhibited fine aerosol (N) emission ratios relative to CO (dN/dCO) of 22.5 ± 9.7 and 23.6 ± 15.1 cm^{-3} parts per billion by volume $(ppbv)^{-1}$ over Brazil and Africa, respectively. Convection coupled with counterclockwise flow around the South Atlantic subtropical anticyclone subsequently distributed these aerosols throughout the remote South Atlantic troposphere. We calculate that dilute smoke from biomass burning produced an average tenfold enhancement in optical depth over the continental regions as well as a 50% increase in this parameter over the middle South Atlantic Ocean; these changes correspond to an estimated net cooling of up to 25 W m^{-2} and 2.4 W m^{-2} during clear-sky conditions over savannas and ocean respectively. Over the ocean our analyses suggest that modification of CCN concentrations within the persistent eastern Atlantic marine stratocumulus clouds by entrainment of subsiding haze layers could significantly increase cloud albedo resulting in an additional surface radiative cooling potentially greater in magnitude than that caused by direct extinction of solar radiation by the aerosol particles themselves.

Introduction

Recently, the effect of atmospheric aerosols on the Earth's radiative budget has received attention as several studies suggest particulate matter contributes a radiative forcing approximately equal but opposite in sign to that produced by the greenhouse gases accumulating within the Earth's atmosphere [*Charlson et al.*, 1992a, b; *Kiehl and Briegleb*, 1993; *Penner et al.*, 1994]. The aerosol forcing is produced by a number of mechanisms. In a direct sense, aerosols reflect solar radiation back into space which increases planetary albedo, hence lowering surface temperatures [*Coakley et al.*, 1983]. Aerosols, particularly the carbonaceous type, also absorb solar radiation [*Ackerman and Toon*, 1981], converting the energy to heat which can modify the temperature lapse rates that govern convective activity and atmospheric dynamics [*Ackerman and Toon*, 1981]. Indirectly, aerosols, in their role as cloud condensation nuclei (CCN), exert a strong influence on a number of cloud radiative parameters as well as the equilibrium of water between the liquid and the gaseous states [*Radke et al.*, 1978]. As evidenced by the increased brightness of clouds formed over well-defined shipping lanes [*Coakley et al.*, 1987], an overabundance of CCN can lead to formation of smaller cloud particles which have, per unit mass, a higher solar reflectivity [*Charlock and Sellers*, 1980; *Twomey et al.*, 1984; *Charlson et al.*, 1987]. CCN concentrations may also effect cloud liquid-water content [*Charlson et al.*, 1987], fractional cloud amount, light absorption by cloud particles [*Twomey*, 1977; *Twomey et al.*, 1984], and rates of precipitation or drizzle [*Albrecht*, 1989; *Radke et al.*, 1990b]. In addition, aerosols influence the abundance of tropospheric greenhouse and other trace gas species through the coupled response of photochemical reaction rates to reductions in shortwave radiation [e.g., Chatfield et al., this issue; *Jacob et al.*, this issue] and increased availability of heterogeneous reaction sites [*Silver e al.*, 1989].

Biomass burning is a prolific source of aerosols to the atmosphere [*Crutzen and Andreae*, 1990] and a region of the world highly effected by this process is the South Atlantic basin, an area which we define, based upon air mass circulation patterns, to include the eastern portion of South America and the western and southern parts of Africa. Here, during the austral winter/spring or "dry season," vast continental regions are burned for agricultural purposes and to clear land to meet increasing population needs [*Crutzen and Andreae*, 1990; *Hao and Liu*, 1994]. Smoke plumes

[1]Atmospheric Sciences Division, NASA Langley Research Center, Hampton, Virginia.
[2]Science and Technology Corporation, Hampton, Virginia.
[3]Aerospace Electronic Systems Division, NASA Langley Research Center, Hampton, Virginia.
[4]Operations Support Division, NASA Langley Research Center, Hampton, Virginia.
[5]Chemistry Department, University of California-Irvine, Irvine.

Copyright 1996 by the American Geophysical Union.

Paper number 96JD00717.
0148-0027/96/96JD-00717$09.00

from these fires are often visible from space [*Wood and Nelson*, 1991; *Cahoon et al.*, 1992] and, at times, reduce visibility so severely in some regions that airports must be closed [*Crutzen and Andreae*, 1990]. In addition, remote satellite measurements have implicated pollution transported from these fires as a factor in causing huge seasonal enhancements in tropospheric O_3 concentrations over the South Atlantic Ocean and neighboring coastal regions [*Fishman et al.*, 1990; *Fishman*, 1991].

Although the local effects of biomass burning in the western tropics have been the subject of several recent investigations [e.g., *Ward et al.*, 1991, 1992; *Andreae et al.*, 1992; *Bingemer et al.*, 1992; *Kaufman et al.*, 1992], the NASA TRACE A mission provided the first opportunity to observe the impact of burning upon tropospheric composition over the entire South Atlantic basin. Conducted aboard the NASA DC-8 aircraft between September 21 and October 26, 1992, near the end of the burning season, TRACE A was coordinated with local air and ground sampling components in Brazil and southern Africa in a multinational effort to characterize the sources, transport, and eventual fate of the fire emissions [*Fishman et al.*, this issue].

Within this report, the DC-8 measurements of 0.1- to 3.0-μm-diameter aerosols are used to evaluate the impact of the burning upon tropospheric aerosol loadings and radiative properties throughout the South Atlantic basin. We begin by surveying the physical characteristics and spatial distributions of aerosols over Brazilian and African source regions, within continental outflow, and over the middle South Atlantic. These results are contrasted with measurements recorded within comparatively unpolluted air masses observed over the North Atlantic to emphasize the relative enhancement of aerosol loadings associated with the biomass burning process. Aerosol emission ratios relative to CO are examined at various locations within the basin in order to evaluate the source strength of the fires and the efficiency with which the aerosols are transported and redistributed within the background troposphere. Finally, to evaluate possible regional scale climate implications, the measured size and spatial distributions are used to calculate the effect of the enhanced aerosols upon atmospheric optical properties and radiative forcing, including the possible affect of the aerosols upon marine stratus-cloud albedo. Companion articles within this issue describe the TRACE A experiment design, the prevailing meteorology, trace gas species emission characteristics of the source fires, the composition of air masses exiting the source regions, and other salient chemical features of air masses sampled by the DC-8 during the experiment [see *Fishman et al.*, this issue for a project overview].

Experiment

The NASA DC-8 aircraft, stationed at Ames Research Center in Moffett Field, California, was used as the primary sampling platform. Flight patterns generally consisted of ramp and spiral profiles punctuated by level altitude runs within the mixed layer (ML) and free troposphere (FT). In general, 4 to 6 constant altitude legs were flown on each intensive sampling mission. Ascent/descent rates during profiles were 150 to 300 m min^{-1}, flight altitudes ranged from 0.3 to 12 km, and nominal airspeeds were ~200 m s^{-1}.

Although the DC-8 carried a large payload of remote and in situ instruments [see *Fishman et al.*, this issue], the CO, CO_2, and lidar measurements are the most pertinent to the following discussions. The CO data were obtained using a differential absorption, tunable diode laser spectrometer (J. E. Collins et al., personal communication, 1996) operated at constant pressure. This system has an accuracy relative to National Oceanographic Atmospheric Association (NOAA) primary calibration standards of 5% (2 σ/average concentration) and precision of 2%. The time constant for TRACE A CO measurements was 2 s to 90% of the final reading. CO_2 mixing ratios were determined using a nondispersive infrared spectrometer [*Anderson et al.*, 1993, 1996] with a precision of ±0.1 parts per million by volume (ppmv), an estimated accuracy relative to the World Meteorological Organization CO_2 standard of ±0.3 ppmv, and a response time of about 2 s. The airborne lidar system provided aerosol distribution information above and below the aircraft, from the surface well up into the stratosphere [*Browell*, 1989]. Aerosol scattering ratios relative to modeled molecular backscatter were recorded for at three wavelengths: 300, 600, and 1064 nm. These measurements have vertical and horizontal resolutions of 60 and 700 m, respectively.

Air mass trajectories were used as a qualitative aid to identify the processes influencing sampled air masses. These were obtained from 5-day backward looking isentropic air mass trajectory calculations based on National Meteorological Center (NMC) wind field grids as described by *Bachmeier and Fuelberg* [this issue]. The general procedure was to calculate the trajectories for a cluster of locations surrounding the point of interest and to only accept those whose groupings that did not diverge considerably during the previous 5 days.

Aerosol number densities and size diameters over the range from 0.1 to 3.0 μm were determined as a function of time using a passive cavity aerosol scattering probe (PCASP) (Particle Measuring Systems, Inc., Boulder, Colorado) which was mounted on a pilon extending 0.5 m below the aircraft's left wingtip, a location calculated to be minimally effected by aircraft-induced flow distortion. The PCASP provides 15 bins of size information, with bins of progressively increasing width (e.g., bin 1 is 0.02 mm wide, whereas bin 15 is 0.5 μm wide). This probe has a resistive heater on the inlet which prevents ice formation during penetration of clouds and acts to dehydrate aerosol samples before measurement [*Strapp et al.*, 1992]. This heater was operated at all times during flight, so that measured number densities and size distributions were unaffected by changes in ambient relative humidity.

The PCASP was calibrated by the manufacturer just prior to the experiment using nonabsorbing, spherical latex particles with real and imaginary refractive indices, n_r and n_i, of 1.59 and 0.0, respectively. This calibration is highly sensitive to deviations of the sampled aerosol optical properties from that of the calibration aerosol [*Kim and Boatman*, 1990]. For example, *Pueschel et al.* [1990] found that sulfuric acid particles with $n_r = 1.44$ were undersized by up to 33% in diameter and an average of 71% in volume by a similarly calibrated optical scattering probe. By inspecting the appropriate Mie scattering curves, we estimate that particles <1 μm in diameter with $n_r = 1.55$ and $n_i = 0.03$ (the values adopted below for biomass burning aerosols) would be undersized by 2 to 3% in diameter resulting in 6–10% and 10–16% underestimates of mass and extinction. However, because the exact composition and hence refractive index of particles sampled during TRACE A is uncertain, we have chosen not to apply corrections to PCASP factory calibration.

Data from the PCASP were recorded at 2 s intervals but have been averaged over varying periods of time for purposes of the following presentation. Total aerosol number densities, N, were obtained by summing the counts from all size bins of the PCASP and are presented, except where specified, in the units of number

per cubic centimeter at standard temperature and pressure (20°C and 760 torr). Particle volumes were calculated by multiplying the number of counts in each size bin of the PCASP by the corresponding bin volume, then summing over all pertinent bins. Particle volume measurements were converted to mass assuming a nominal aerosol mass density of 1.0 g cm^{-3} [*Radke et al.*, 1988].

Regression statistics for the relationship between CO_2 and aerosols and CO in haze layers and plumes are presented in the following tables and discussions. Because of the large number of cases, rather than editing and extracting the individual data segments for analysis, we calculated "running", 30-point (5 min) linear regressions with 25-point overlap on the entire data. Time series exhibiting CO standard deviations > 5 ppbv were judged to contain plumes, and statistics for only such series with r^2 values between the variables of interest exceeding 0.45 ($p > 0.99$) were used in preparing the tables and figures.

Optical properties of aerosols were calculated using a standard Mie scattering algorithm for spherical particles as described by *Bohren and Huffman* [1983]. This calculation is highly sensitive to the value selected for the index of refraction, and a wide range of values have been reported for the 500- to 550-nm wavelength (e.g., solar maximum) region for biomass burning aerosols. This parameter is comprised of two terms. The real part, n_r, which controls loss due to scattering, has been estimated to lie between 1.38 and 1.55, with the majority of values grouped between 1.52 and 1.55 [*Li and Mao*, 1990; *Lenoble*, 1991; *Westphal and Toon*, 1991]. We have chosen to make our calculations using the value of 1.55. A sensitivity study indicates that if 1.52 were correct instead of 1.55, the scattering would decrease by 6%. The imaginary term, n_i, reportedly varies from 0.01 to 0.04 [*Li and Mao*, 1990; *Lenoble*, 1991; *Westphal and Toon*, 1991]. We have, based on the reported fraction of elemental carbon in tropical biomass burning aerosols [*Andreae et al.*, 1988], chosen to use 0.03 in our calculation. This gives a single-scatter albedo, $\omega(\tau_a/\tau_e$, where τ_a is the aerosol absorption and τ_e is the aerosol extinction), of about 0.83. In addition, we note that a variation of n_i from 0.03 to 0.015 increases the scattering by 5%, since the absorption decreases.

The Mie scattering calculation is very sensitive to aerosol size diameter. Thus because biomass burning aerosols are reportedly fairly active CCN [e.g., *Radke et al.*, 1978, 1991], we must also assume that their size varies as function of relative humidity (RH) [e.g., *Fitzgerald*, 1975; *Winkler*, 1988; *Hagen et al.*, 1989]. To make this correction and because suitable information for biomass burning aerosols were lacking, we used the RH growth curve for large continental particles given in Table 2 of *Winkler* [1988]. These data indicate that the size of hygroscopic particles are relatively unchanged at RH < 50% but undergo gradual growth at higher humidities, reaching $r/r_o = 1.77$ for 97.5% RH. Corresponding refractive indices were adjusted by linearly interpolating between the value for dry combustion aerosol and that for pure water (1.33–0i) based on the fraction of water contained within the humidified particle. Because of the very dry conditions over the eastern South Atlantic basin, application of the RH correction made little difference to the calculated optical properties of the African aerosol but, due to the greater prevalence of wet convection and moisture associated with the ending of the dry season in the western tropics, increased column-integrated extinctions by up to 40% for some of the Brazilian cases.

A map of the study area with overlying paths for the southern hemispheric flights is shown in Figure 1. The takeoff and landing sites and times along with the individual mission objectives are given by *Fishman et al.* [this issue]. Briefly, missions 3, 4, 18, and 19 were transits to and from the experiment area and included encounters with both clean North Atlantic and smoke-tainted South Atlantic air masses. Flights 5 and 8 and 13, 14, and 15 investigated continental outflow over the Atlantic from Brazil and Africa, respectively. Missions 6 and 7 over Brazil and 10 and 12 over south central Africa focused upon obtaining source emission signatures for the two source regions. Flight 17 and portions of 16 and 18 were conducted near Ascension Island to examine the impact of biomass burning upon the composition of remote South Atlantic air masses.

Results and Discussion

Large-Scale Observations

The TRACE A field deployment took place between September 21 and October 26, 1992, near the end of the burning season over both continents. At that time, fire count statistics indicate burning activity was greatly reduced in Brazil because of rainy weather over the interior agricultural regions [*Fishman et al.*, this issue]. Also, a severe draught over southern Africa had limited the growth of vegetation, so that only a fraction of normal fuel was available for combustion [*Bachmeier and Fuelberg*, this issue]. However, despite this reduced frequency of fires, fine aerosol number densities were greatly enhanced, particularly within the middle to upper troposphere, over the entire tropical/subtropical South Atlantic basin relative to northern hemisphere observations (Figures 2 and 3). Indeed, a rough comparison of Figure 2 data suggests that values at altitudes above the marine boundary layer were at least an order of magnitude greater over the southern regions. These loadings, which are also approximately a factor of 10 higher than seen during the wet season over coastal and interior Brazil [*Gregory et al.*, 1990], are consistent with previous South Atlantic dry season observations [*Anderson et al.*, 1993a; *Andreae et al.*, 1994] and are supported by simultaneous observations of high concentrations of other pyrogenic pollutants and photochemically produced O_3 [*Blake et al.*, this issue; *Gregory et al.*, this issue; *Smyth et al.*, this issue; *Talbot et al.*, this issue]. Meteorological analyses [*Bachmeier and Fuelberg*, this issue; *Fuelberg et al.*, this issue; *Pickering et al.*, this issue] and examinations of chemical signatures [*Talbot et al.*, this issue] suggest that the primary source of this pollution was biomass burning over South America and Africa.

Aerosol Sources and Characteristics

At the time of TRACE A the regions of most intense burning were located between 5°S to 15°S over the cerrado of northeastern Brazil and between 5°S and 25°S over the savannas of eastern Africa. Burning in both locations was mainly related to clearing of grass/shrub land to stimulate growth of new grasses or in preparation of planting agricultural crops. Smoldering burn scars observed over Brazil were, in general, widely distributed and relatively small in aerial extent (a few hectares), whereas over Africa, fire lines hundreds of meters long attached to large scars (many square kilometers) were greatly in evidence. In both regions the whitish gray smoke from the fires produced widespread haze and reduced visibility [*Kirchhoff et al.*, this issue; *Le Canut et al.*, 1996].

The aerosol and chemical [*Blake et al.*, this issue] signatures of smoke palls over Brazilian and African source regions were quite similar. Indeed, volume density curves from both areas

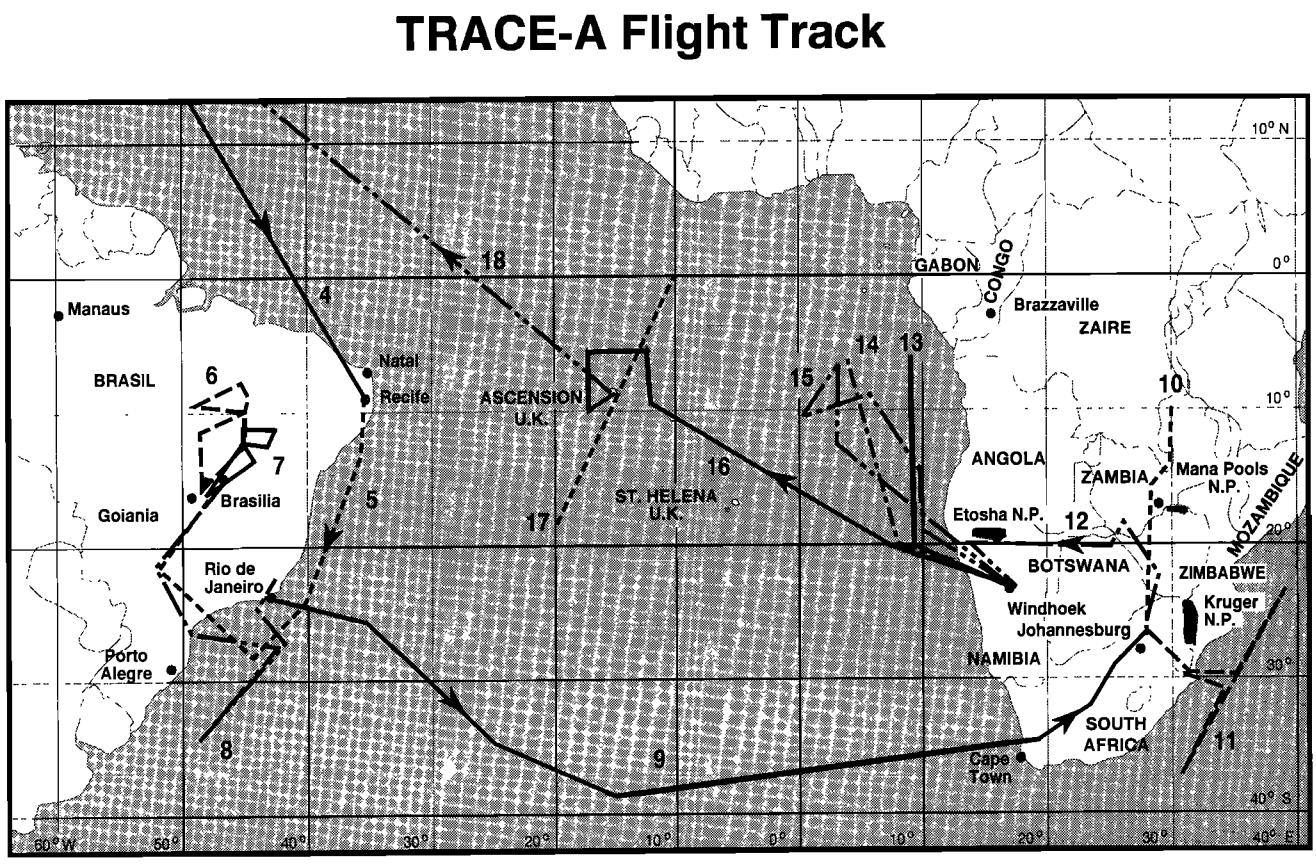

Figure 1. TRACE A experiment area and flight tracks.

show evidence of modes at ~0.25, 1, and >3 μm (Figure 4). The 0.25-μm peak corresponds to accumulation mode aerosols which reportedly compose the largest mass fraction of particle flux from vegetation fires [*Le Canut et al.*, 1996]. These particles, a primary combustion product [*Radke et al.*, 1991], displayed only a slight tendency to increase in size with age. Indeed, inspection of individual 10-s-averaged volume size distributions suggest the accumulation mode peak ranged only from diameters of 0.2 to 0.275 μm. Aerosols comprising the ~1- and >3-μm modes

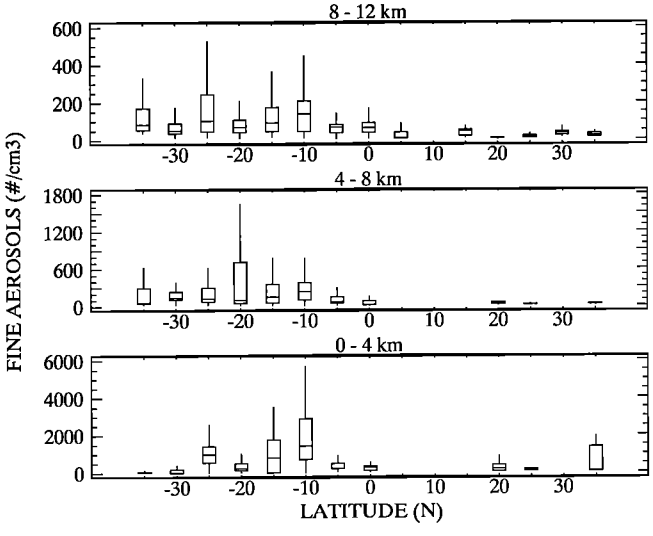

Figure 2. Distribution of aerosol number density as a function of latitude during the TRACE A field experiment. In these multiple "box and whisker" type plots the horizontal lines represent mean values, the boxes enclose the middle 50% of the data, and the vertical lines extend either over the entire data range or to a maximum of 1.5 times the inner-quartile distance. The data are grouped according to altitude and without regard to location or flight, although measurements recorded within clouds or on takeoffs and landings were deleted.

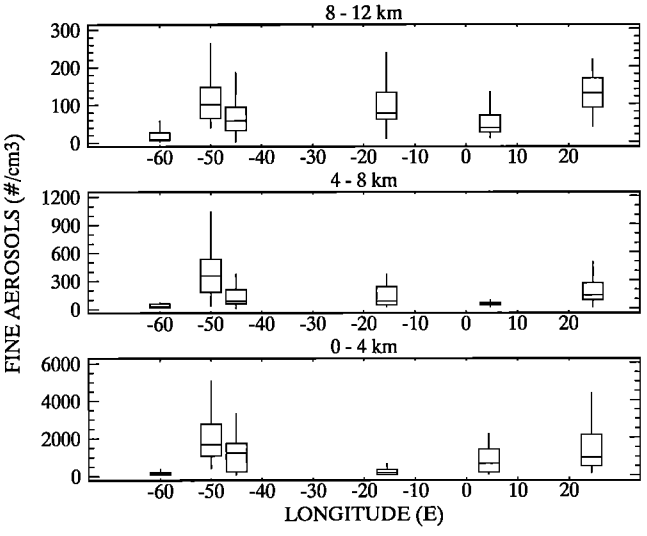

Figure 3. Distribution of aerosol number density as a function of longitude during the TRACE A field experiment. The data centered at −60° represents the North Atlantic (NA) tropics, whereas those at −50°, −45°, −15°, 5°, and 25° are for the Brazil source (BS), Brazil outflow (BO), middle South Atlantic (MSA), African outflow (AO), and African source (AS) regions, respectively. See Figure 2 for an explanation of the plot format.

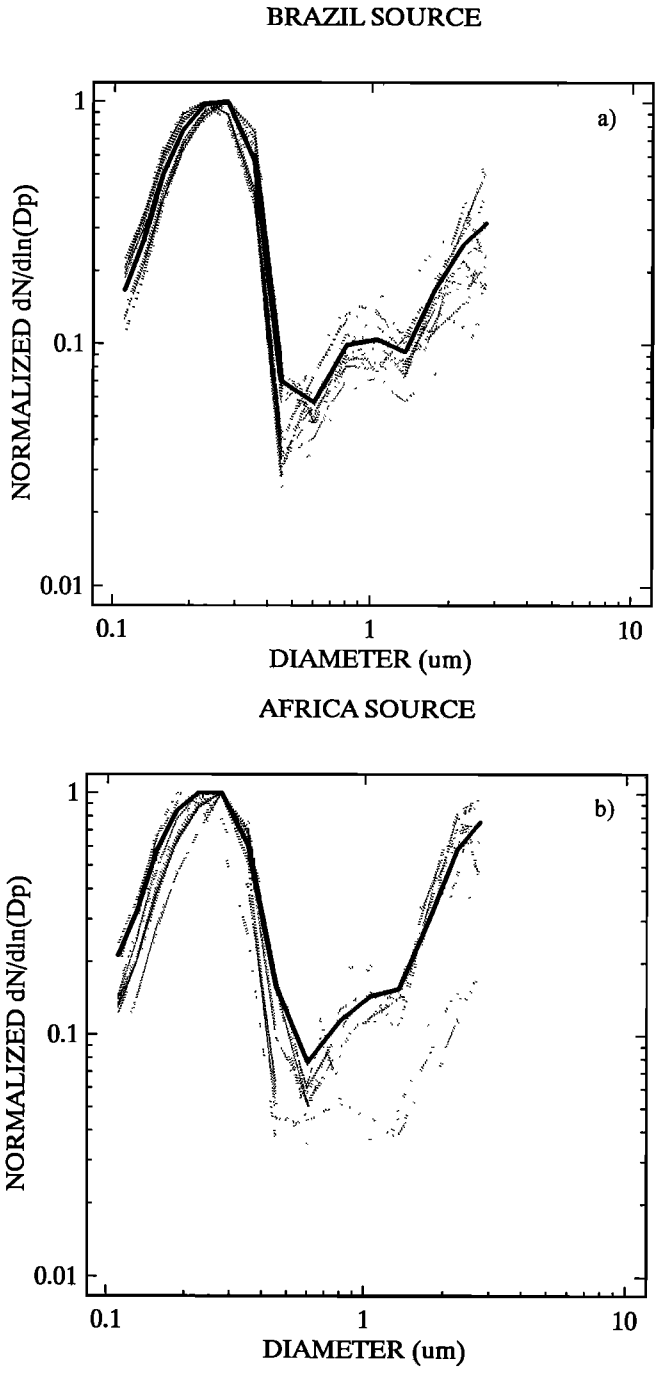

Figure 4. Five-minute-averaged peak-normalized volume density size distributions for biomass burning aerosols observed within smoke palls over (a) Brazilian and (b) African source regions. The solid lines in each plot represents the grand average of the presented distributions.

(Figure 4) were apparently not primary combustion products as neither displayed significant correlation with CO (a combustion tracer) in regressions of 10-s averaged data. However, a compilation of aerosol mass concentration statistics for background ($N < 500$ cm^{-3}) and smoke-tainted air ($N > 1000$ cm^{-3}) (Table 1) suggests the medium and large particles were present in higher concentrations within burning-influenced air. We suspect these modes were comprised of ash or soil particles suspended by atmospheric dynamics related to the fires. Note that in many

Table 1. Size Dependent Mass Concentrations (μg/m^3) for Relatively Clean and Smoke-Polluted Boundary Layer Airmasses over Brazil and Africa

	Aerosol Mass (μg/m^3)																	
	Total (0.1–3.0 μm)				Small (0.01–0.9 μm)				Medium (0.9–1.5 μm)				Large (1.5–3.0 μm)					
Air Mass	min	max	avg	s.d.	min	max	avg	%tot	s.d.	min	max	avg	%tot	s.d.	min	max	avg	%tot	s.d.
Brazilian smoke	3.5	74.3	12.6	8.3	3.4	62.5	10.6	84	7.0	0.0	3.4	0.5	4	0.4	0.0	65.0	1.5	12	3.0
Brazilian background	2.0	5.1	3.5	0.8	0.2	1.7	2.3	67	0.2	0.0	1.4	0.3	9	0.2	0.0	2.4	0.9	26	0.8
African smoke	1.2	119.0	25.2	23.6	1.2	114.0	21.7	86	21.0	0.0	3.5	0.7	3	0.6	0.0	15.1	2.8	11	2.7
African background	0.4	9.3	2.2	2.0	0.4	2.2	1.0	46	0.5	0.0	1.1	0.2	9	0.3	0.0	7.8	1.0	45	1.6

Values have been adjusted to standard temperature and pressure (20°C and 760 torr).

cases, coarse aerosol loadings were slightly greater over Africa than Brazil (see Figure 4). There, meteorological and soil moisture conditions in the savanna regions were extremely dry which suggests that winds and convection associated with the fires could have suspended soil particles. It is also likely that the burning ground cover was coated with a fine layer of soil particles which were subsequently entrained within rising smoke plumes.

Returning our focus to the accumulation mode particles (0.1 to 0.9 μm), over continental source regions, we observed number densities within relatively dilute emissions (CO < 1000 ppbv) sampled at >0.3 km above ground level (AGL) that often exceeded 10,000 cm^{-3} as compared to 300–500 cm^{-3} in "background" air. The variations in the number (N) and mass (M); (calculated assuming a density of 1.0 g cm^{-3} based on compositional measurements of dry biomass burning particles by *Andreae et al.* [1988]) concentrations of these particles were highly correlated with the mixing ratio of combustion tracers (Figures 5a and 5b). That the changes in aerosol concentration bear a closer relationship to CO than CO_2 (Figure 5c) suggests the unit production of fine aerosols is, like CO formation, inversely proportional to burning efficiency, thus more such particles are formed per unit of fuel consumed during the smoldering than open flame stages of fires.

The high positive correlation observed between aerosol number and mass concentrations and CO allows us to calculate source emission ratios for these parameters. Table 2 presents concentrations and emission ratios of N and M relative to CO for planetary

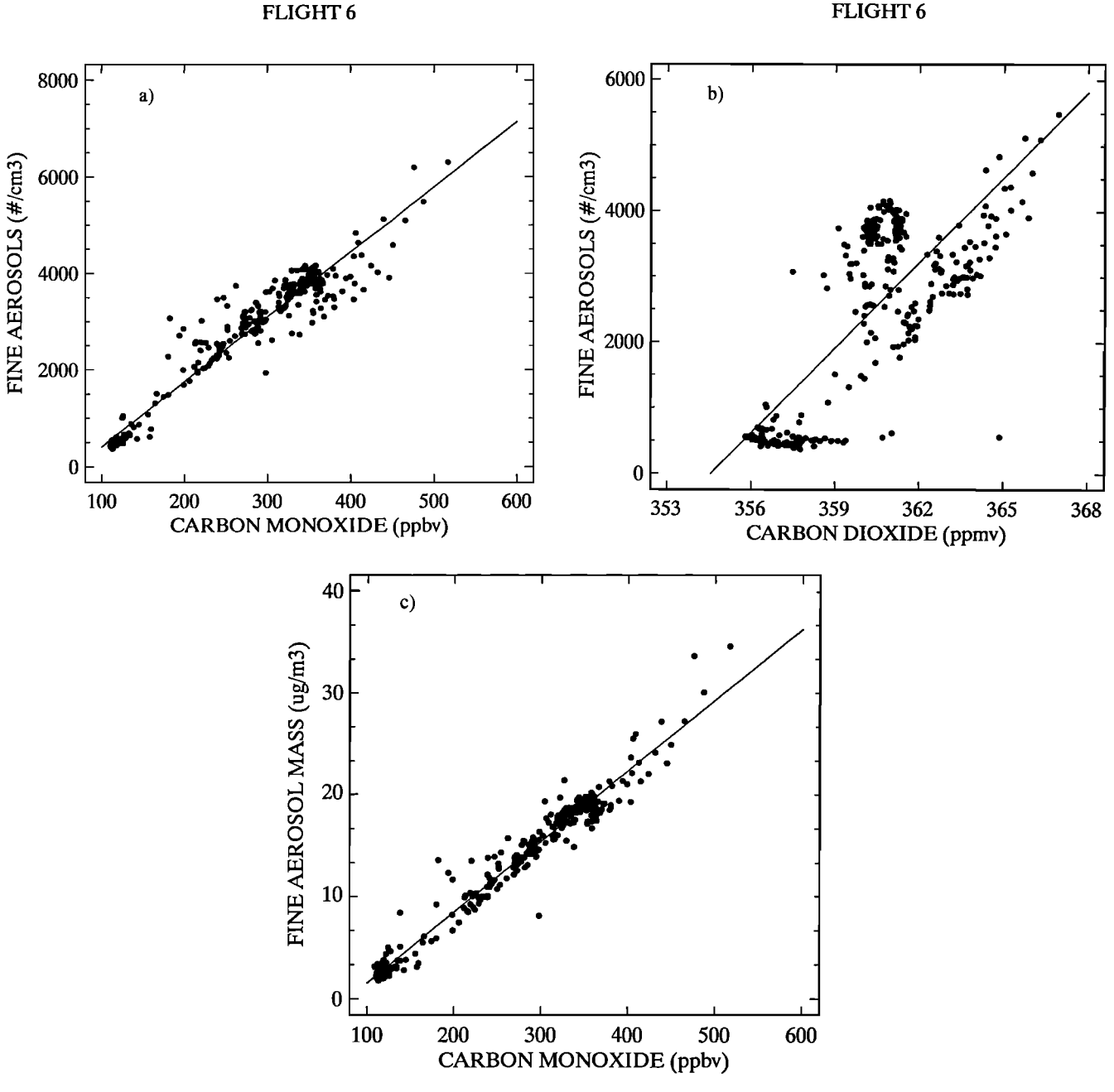

Figure 5. Scatter diagrams of (a) N versus CO, (b) N versus CO_2, and (c) M versus CO prepared from 10-s-averaged data recorded on flight 6 during a low-altitude pass over Brazilian vegetation fires.

Table 2. Statistics for Mixed Layer Flight Legs Over Brazilian and African Source Regions

Parameter	Number of Points	Minimum Value	Maximum Value	Median Value	Average Value	S. D.
			Brazil			
CO, ppbv	1110	109	1420	179	207	102
CO_2, ppmv	1088	355.1	386.1	360	359.5	2.8
N, cm^3	1254	406	18000	1880	2220	1490
M, $\mu g/m^3$	1254	1.9	62.8	7.1	9.4	7.2
dN/dCO, cm^3/ppbv	117	5.5	61	24	22.5	9.7
dM/dCO, $\mu g/m^3$/ppbv	117	0.017	0.264	0.072	0.081	0.040
dCO/dCO^2, ppbv/ppmv	76	9	79	26	29	12
			Africa			
CO, ppbv	713	72	1130	99	148	129
CO_2, ppmv	668	354.8	371.7	357.2	358.1	2.3
N, cm^3	922	92	19500	936	2140	3150
M, $\mu g/m^3$	922	0.26	96.8	3.8	9.4	14.9
dN/dCO, cm^3/ppbv	24	5.4	54	21	23.6	15.1
dM/dCO, $\mu g/m^3$/ppbv	24	0.008	0.200	0.091	0.102	0.065
dCO/dCO^2, ppbv/ppmv	19	10	70	14	27	20

boundary layer (PBL) (the lowest 1–2 km above ground level) measurements over the Brazilian and African source regions. The peak aerosol number density and mass mixing ratios reported in the table are consistent with African savanna fire data collected at nearly the same time by European investigators during Southern African Fire—Atmosphere Research Initiative, September-October 1992 (SAFARI 1992) [*Le Canut et al.*, 1996].

Using the formula adopted by *Le Canut et al.* [1996] and the dCO/dCO_2 values of Table 2, we calculate that the combustion efficiencies of emissions sampled over both locations ranged from about 91 to 99%, which suggests the respective source fires were generally in the flaming stage of combustion. Aerosol emission ratios relative to CO, dN/dCO, varied from 5.5 to 61 cm^{-3} $ppbv^{-1}$ over Brazil and 5.6 to 54 cm^{-3} $ppbv^{-1}$ over Africa. For comparison, *Le Canut et al.* [1996] report average dN/dCO values for southern African grassland/savanna fires observed during the same time period ranging from about 14 to 57 cm^{-3} $ppbv^{-1}$. Several of the lower dN/dCO values over Brazil were observed just below cloud base in plumes that may have been previously cycled through clouds. Indeed, as described below, such values were common in the upper troposphere and *Andreae et al.* [1994] report an average dN/dCO of 5.2 ± 1.7 cm^{-3} $ppbv^{-1}$ for aged plumes sampled above cloud level over the western tropical Atlantic during the dry season of 1989. Mean and median dN/dCO were very similar for the African and Brazilian fires and the slight difference evident in the submicron aerosol mass emission ratios, dM/dCO, was not statistically significant. The observed dM/dCO values, 0.08 ± 0.04 μg m^{-3} $ppbv^{-1}$ for Brazil and 0.102 ± 0.065 μg m^{-3} $ppbv^{-1}$ (at standard temperature and pressure), lie at the middle to low end of the range reported by previous investigators [*Andreae et al.*, 1988; *Ward et al.*, 1990, 1991, 1992; *Radke et al.*, 1991]. For a more direct comparison, *Le Canut et al.* report values for this ratio for 0.1- to 3.0-μm particles assuming a 1.0 μm cm^{-3} mass density ranging from about 0.036 to 0.210 ng m^{-3} ppbv for fires within equivalent African ecosystems sampled at the time of TRACE A; we estimate that our dM/dCO values would increase by ~20% if 1- to 3-μm particles were included in the mass calculations (see Table 1).

Aerosol Transport

Vertical redistribution. The fate of the aerosol emissions and their impact on regional processes is highly dependent upon the meteorological environment into which they are introduced. During the time of TRACE A, subsidence and the absence of available water vapor limited the vertical extent of convection over African fire regions. In contrast, the dry season was ending over Brazil and frontal systems spawning thunderstorms frequently propagated through the central burning areas [*Bachmeier and Fuelberg*, this issue]. The greater prevalence of deep convection in Brazil was reflected in the higher and more variable concentration of CO over the region as compared to Africa at altitudes >4 km (Figure 6a). Aerosol profiles (Figure 6a) provide further evidence that vertical transport was more efficient within the Brazilian regime as values above 6 km were, in general, a factor of 2 greater there than over Africa. However, note that even over Africa, the cleanest layers generally contained ~10 times more aerosols than recorded within North Atlantic and U.S. continental air masses observed during TRACE A ferry flights (Figures 2 and 3).

Moreover, a comparison between the N and CO profiles suggests that a considerable portion of the smoke particles were lost during the vertical transport process (Figure 6a and 6b). This was not due to humidity effects on the measurement, e.g., a reduction in aerosol diameters below the instrument's size range sensitivity, because, as noted above, the PCASP probe has deicing heaters which dry the particles prior to measurement. More likely, the aerosols were scavenged by precipitation during passage through convective clouds [*Chuang et al.*, 1992]. Most biomass burning aerosols contain a large fraction of soluble material [*Andreae et al.*, 1988] and reportedly make quite active CCN [*Radke et al.*, 1978, 1991]. Vertical profiles of dN/dCO (Figure 6c) over both

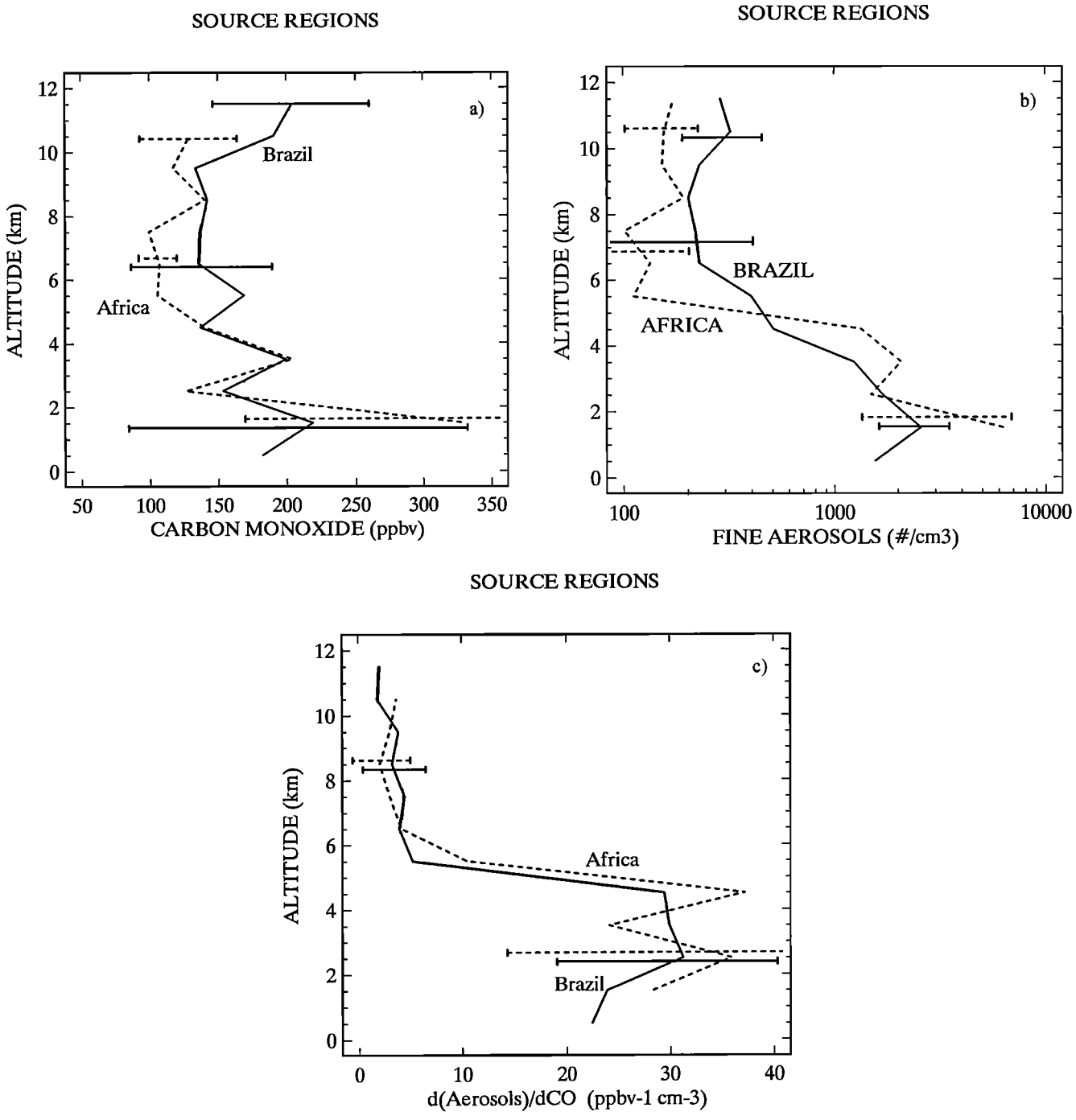

Figure 6. Average vertical profiles of (a) CO, (b) N, and (c) dN/dCO over Brazilian and African source regions as defined within the text. The error bars represent the average value $\pm 1\sigma$.

regions reach a maximum at the top of the PBL (~4 km) and fall precipitously in going to higher altitudes. In the Brazilian case, the ratio averages 24.5 ± 10.5 cm^{-3} $ppbv^{-1}$ below 4 km and 2.9 ± 1.4 cm^{-3} $ppbv^{-1}$ above 6 km; over Africa the values are 25.7 ± 18.3 and 4.2 ± 3.5 cm^{-3} $ppbv^{-1}$, respectively. The high-altitude dN/dCO ratios are not statistically different between the two locations in spite of the fact that, in general, middle to upper tropospheric air masses over Brazil had been subjected to more recent pollution input than those sampled over Africa [*Bachmeier and Fuelberg*, this issue; *Talbot et al.*, this issue]. Indeed, many fairly fresh (<2 days old [*Fuelberg et al.*, this issue]) haze layers sampled within convective outflow over Brazil exhibited ratios of <2 cm^{-3} $ppbv^{-1}$, which implies that their submicron aerosol content had been reduced by up to 90% or more, presumably by precipitation scavenging. This, coupled with the fact that, as discussed later, dN/dCO at upper elevations did not vary significantly with location over the entire South Atlantic basin, suggests that cloud processing at low to midtropospheric levels was the primary loss mechanism for fine aerosols and also that the lifetime of aerosols within the upper troposphere was of the same order as that for CO.

Continental outflow. During the austral winter/spring the

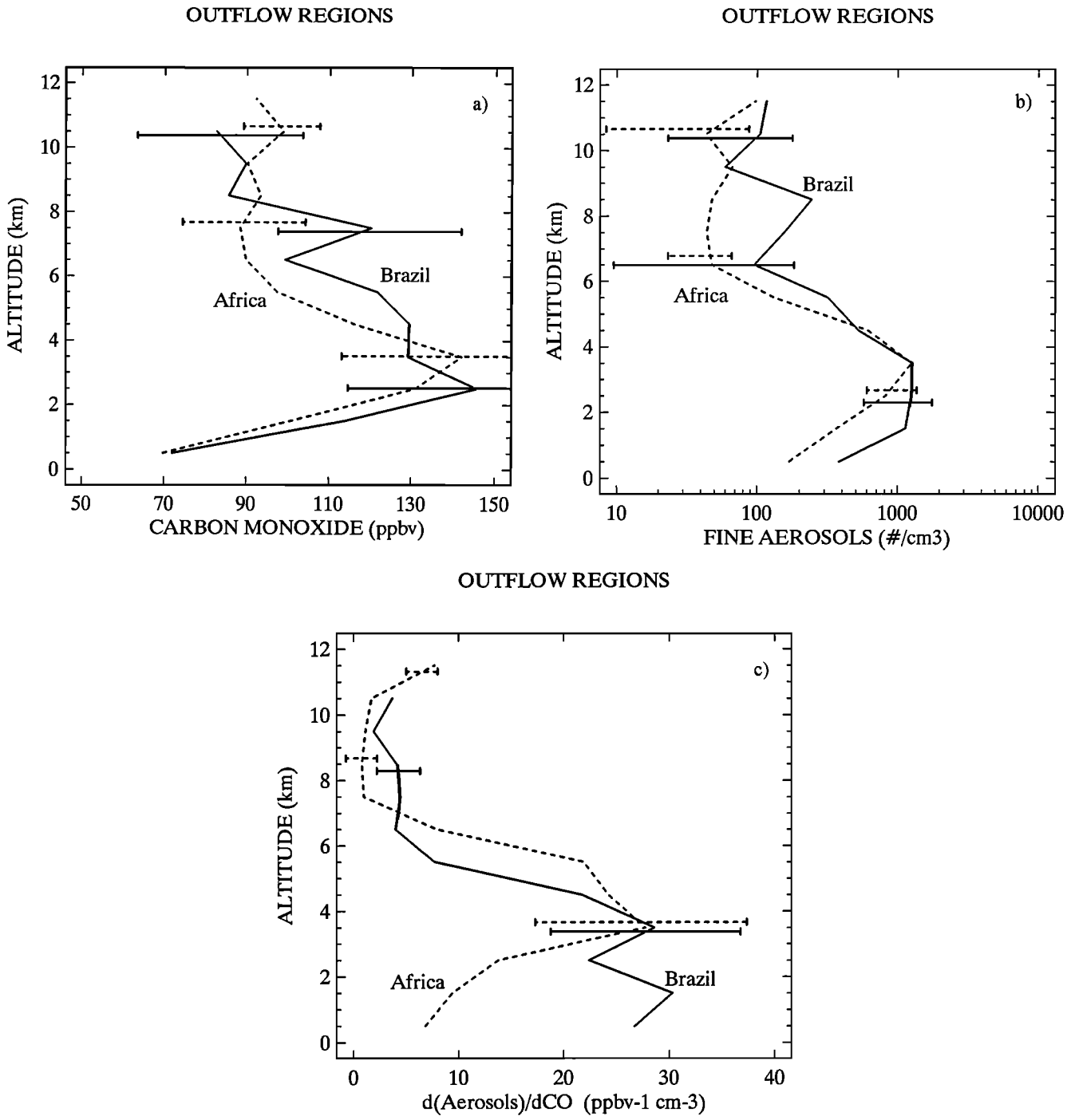

Figure 7. Average vertical profiles of (a) CO, (b) N, and (c) dN/dCO over Brazilian and African continental outflow regions as defined in the text. The error bars represent the average value $\pm 1\sigma$.

South Atlantic subtropical anticyclone often couples with continental anticyclones to form a large circular flow pattern bounded on the east and west by mountain ranges over Africa and South America and to the north and south by the Intertropical Convergence Zone (ITCZ) and subtropical jet, respectively. In general, north of the ridge axis, air is exhausted off Africa and transported over the Atlantic by trade winds in the direction of South America, whereas south of the axis, South American air is propagated toward Africa [*Bachmeier and Fuelberg*, this issue].

Data obtained over coastal regions on flights 4, 5, and 8 and 13, 14, 15, and 16 suggest air exhausted off both Brazil and southern Africa, respectively, were highly contaminated with biomass burning emissions [*Bachmeier and Fuelberg*, this issue; *Blake et al.*, this issue; *Gregory et al.*, this issue; *Talbot et al.*, this issue]. Peak pollutant concentrations were generally found between 2 and 6 km in both cases (Figure 7). Although chemical and meteorological analyses suggest the African outflow was several days farther removed from source regions, aerosol concentrations within this peak outflow band remained quite high in both regimes and, for the most part, relatively unchanged in relation to the concentrations of more conserved species. For the two cases, average aerosol number densities at 3 to 4 km were

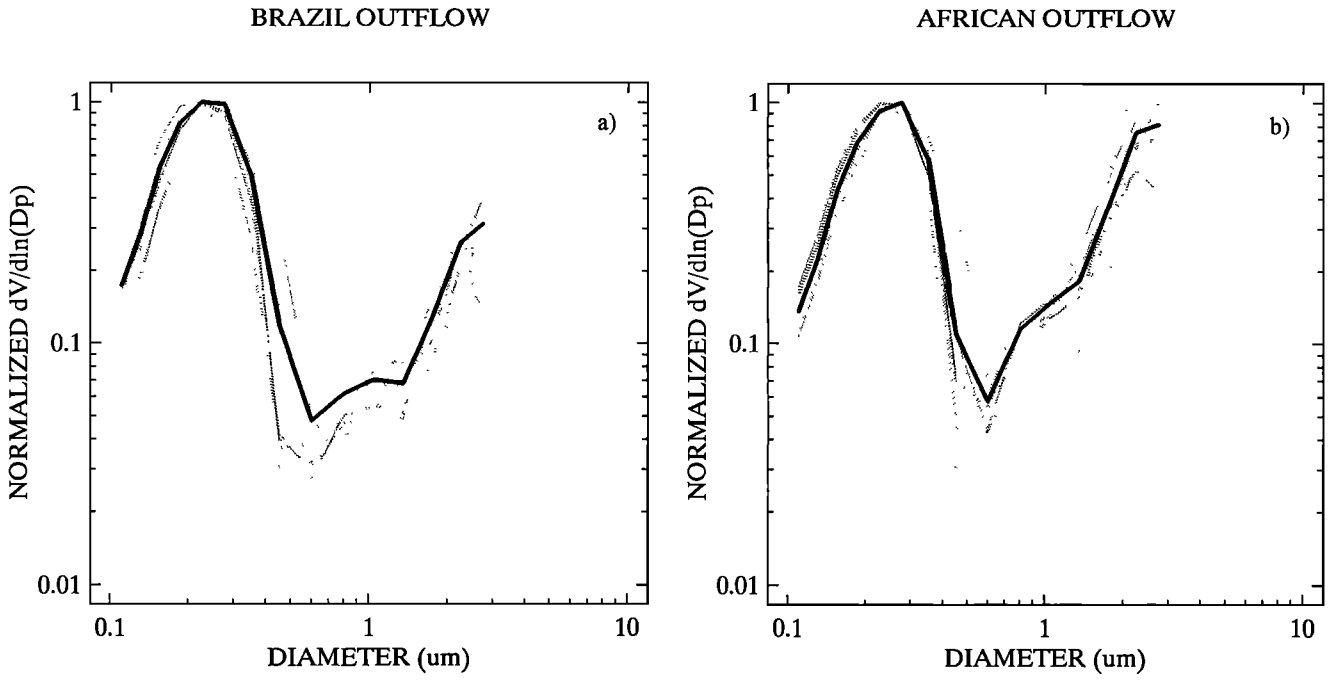

Figure 8. Five-minute-averaged peak-normalized volume density size distributions for biomass burning aerosols observed within (a) Brazilian and (b) African continental outflow at approximate 3 km altitude. The solid lines in each plot represent the grand average of the presented distributions.

~1000 cm^{-3} and dN/dCO ratios were ~25 cm^{-3} $ppbv^{-1}$, which is about the same as seen over continental source regions (Table 2), suggesting very little aerosol is lost during horizontal transport within this preferred outflow band.

Aerosol size distributions within continental outflow (Figure 8) were very similar to those recorded over source regions (Figure 4). In fact, close inspection reveals that the African volume spectra are almost identical despite the large difference in time since emission (several days). As to the Brazilian data, the accumulation mode peak remains at the same diameter but is somewhat broadened. Also, a slightly greater volume of aerosols are found at diameters >0.7 μm which is likely related to the sampling of African emissions along the northern portion of the flight tracks on flights 4 and 5.

Long range effects. Streamline and trajectory analyses indicate air sampled in the region around Ascension Island arrived from diverse locations, depending on altitude and position relative to the island. At high elevations, air along most flight paths origi-nated over South America, whereas near the surface, clean mari-time air from the subtropical South Atlantic was prevalent. Air at midlevels (~2 to 6 km) appeared to originate over southern Africa although most 5-day backward trajectories (the limit of our cal-culations) fell short of reaching the continent.

Because of these convoluted flow patterns, trace species concentrations exhibited wide ranges of values over the region. For example, CO varied from ~70 to 140 ppbv and average 90 ppbv at 2.5 km altitude (Figure 10a). Similarly, N values at that height ranged from ~30 to >1000 cm^{-3} and averaged ~200 cm^{-3} (Figure 10a). (For comparison, during the summer 1989 NASA/CITE 3 airborne field experiment, we observed N values averaging only 640 cm^{-3} within visibly hazy continental outflow some 50 km downwind of the U.S. East Coast [*Anderson et al.*, 1993b].) The lowest values were seen in air arriving from higher latitudes of the South Atlantic, whereas the higher pollutant concentrations were found in haze layers which meteorological and chemical analyses indicate originated over southern Africa, possibly >1 week earlier. These layers were rich in CH_3Cl, a biomass burning tracer and, as was the case for African outflow, were generally confined between the trade wind inversion and a more elevated subsidence-related inversion [*Talbot et al.*, this issue]. Aerosol size distributions (Figure 9) within these pollution layers were quite similar to those recorded over and downwind of African biomass burning areas. We conclude from this observation that the African biomass burning aerosols underwent little physical change during westerly transport, which is most likely due to the virtual absence of midlevel clouds along the path.

It also appears that the low-level haze layers lost little of their aerosol content during the transport process (Figure 10). The value of dN/dCO observed between 2 and 4 km altitude ranged up to 31 and averaged 17.6 ± 6.6 cm^{-3} $ppbv^{-1}$ in layers containing ≥5 ppbv CO enhancements; mass ratios, dM/dCO, averaged 0.082 ± 0.011 μg m^{-3} $ppbv^{-1}$ for these cases. These values are not statistically different than those observed directly over savanna fires (Table 2).

TRACE A observations suggest that the freshest and, from a trace gas standpoint, most significant inputs of pollution to the middle South Atlantic occurred within the middle to upper troposphere (Figure 10a and 10b); [*Smythe et al.*, this issue; *Talbot et al.*, this issue]. These upper level enhancements are particularly evident when compared to corresponding concentrations measured within the aged tropical North Atlantic air masses encountered on flights 4, 18, and 19. For example, at 8 km, average CO and N values were, respectively, ~50% and 8 times greater over the southern than over the northern tropics. Back trajectory analyses suggest that in many cases this upper level pollution was embedded within westerlies which had recently passed through regions of convection over equatorial South America. The exact origin(s) of these parcels is/are uncertain, but all contained low levels of urban tracers (e.g., C_2Cl_4, see

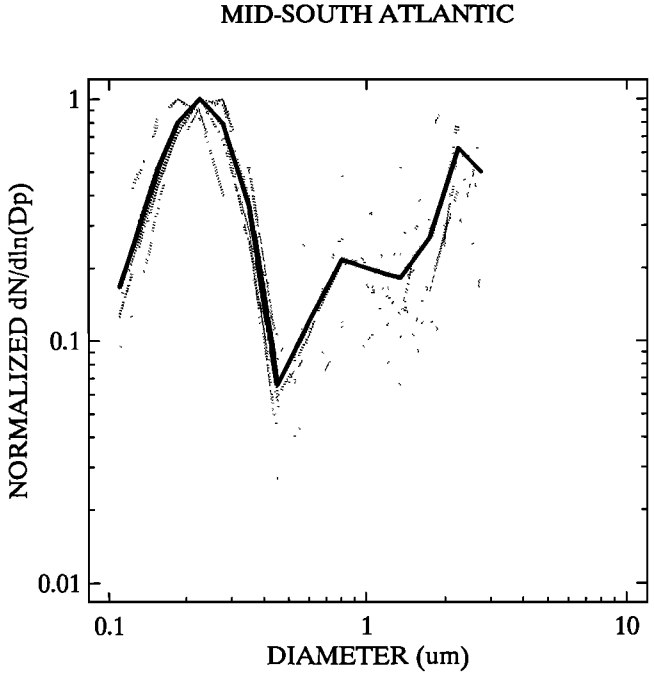

Figure 9. Five-minute-averaged peak-normalized volume density size distributions for biomass burning aerosols observed within a low-level haze layer over the South Atlantic in the vacinity of Ascension Island. The solid line represents the grand average of the presented distributions.

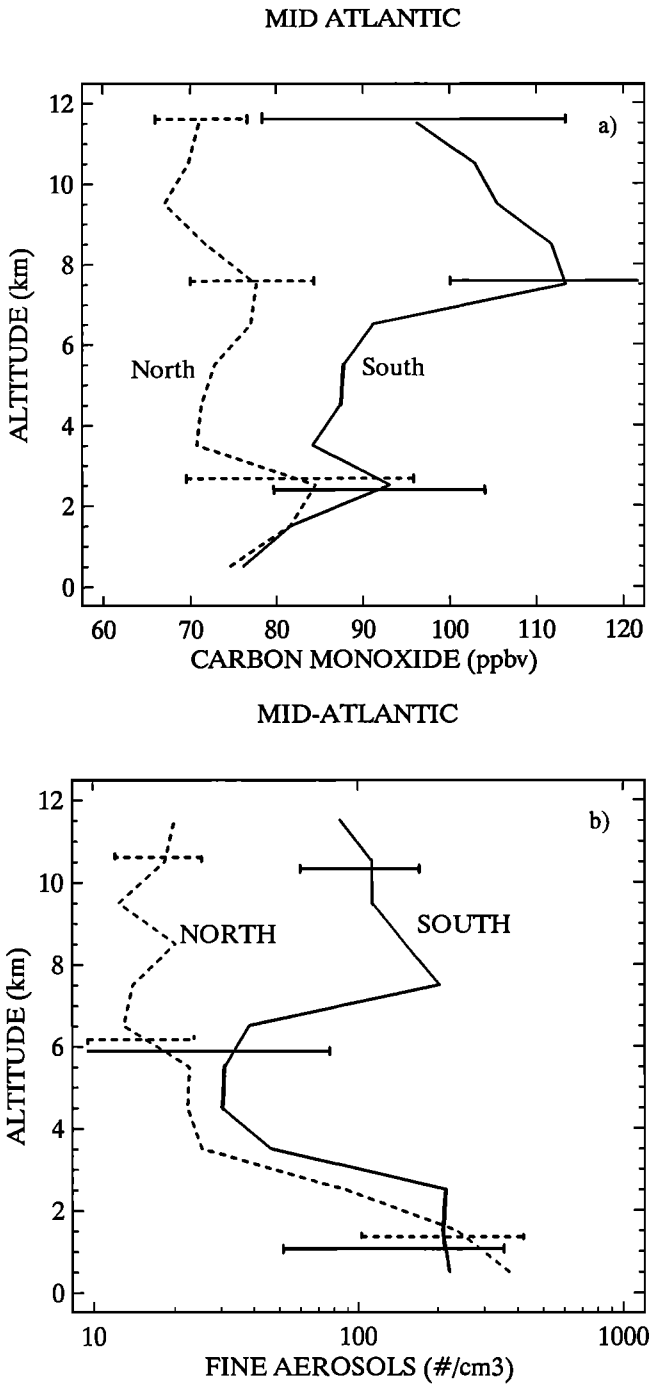

Figure 10. Average vertical profiles of (a) CO, (b) N, and (c) dN/dCO over the central South Atlantic region near Ascension Island. The error bars represent the average value $\pm 1\sigma$.

Blake et al., [this issue]) and most were enriched in CH_3Cl indicating possible contamination from biomass burning emissions [*Smythe et al.*, this issue]. Aerosol number density variations within these layers were highly correlated with that of CO which suggests they arose from a combustion source. Thus although other sources are quite feasible, to simplify subsequent analyses, we will ascribe the same physical properties to these particles as assumed for the biomass burning aerosols.

Impact on Tropospheric Optical Properties

The above sections suggest that biomass burning led to enhancements in aerosol number densities over all regions of the South Atlantic basin visited during TRACE A. To evaluate the radiative impact of these aerosols, we have used a standard single-scatter, Mie algorithm [*Dave*, 1968; *Wiscomb*, 1980; *Bohren and Huffman*, 1983] to calculate aerosol optical properties for selected individual and average vertical soundings. To make the problem more tractable, we assumed that aerosol loadings at all locations were dominated by biomass burning particulates and that particles of all sizes were of uniform composition and spherical shape (see experimental section above for further details). Although comparisons between calculated and lidar-observed aerosol extinction profiles were generally quite good, we estimate that these assumptions coupled with uncertainties in refractive index and probe calibration produce a maximum uncertainty of ±50% in the calculated optical properties.

Sample results are seen in Figure 11 for a profile recorded through a regional smoke pall over African savanna on flight 10. Simultaneous meteorological soundings (not shown) indicated that inversions at 2.5 and 4 km, a wet layer between 6.5 and 7.5 km altitude, and that, within 50–100 m below the higher inversion, RH exceeded 90%. Aerosol number densities (Figure 11a) were quite high throughout both the surface-based and the secondary mixed layer as values between 3000 and 10,000 cm^{-3} (uncorrected for temperature and pressure) at altitudes below 4 km were common. RH-corrected aerosol mass densities (Figure 11b), calculated from individual 10-s-averaged size distributions, averaged ~40 $\mu g\ m^3$ and reached a peak of 80 $\mu g\ m^{-3}$ in the humid layer at 4 km. Aerosol number and corresponding mass densities decreased 1 to 2 orders of magnitude above the 4-km inversion, reaching a mini-

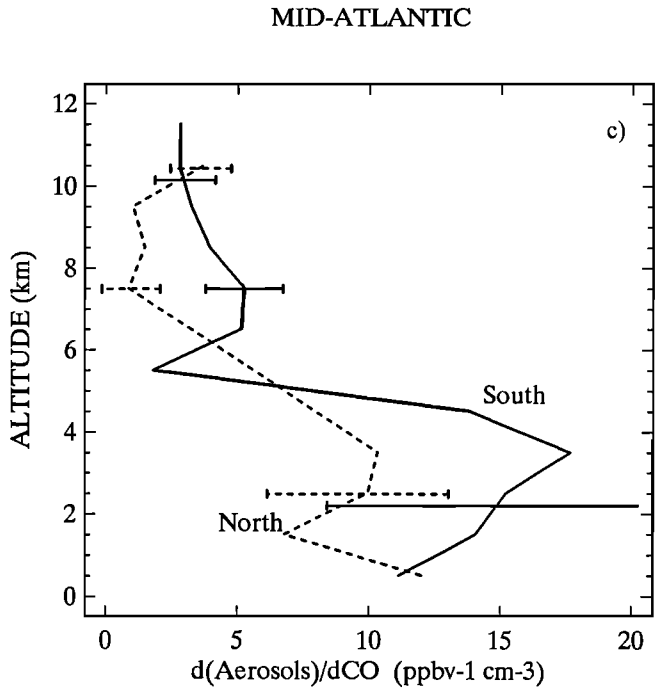

Figure 10. (continued)

mum at 7 km. The calculated 500-nm optical attenuations (Figures 11c–11e) mimic the aerosol distribution, exhibiting large values below 4 km and correspondingly smaller values above.

The vertical optical attenuation profiles (i.e., Figures 11c–11e) can to be integrated as a function of altitude to obtain depths for extinction, absorption, and backscatter. Performing this operation on Figure 11 data yields values of 0.71, 0.09, and 0.009 for τ_{ext}, τ_{abs}, and τ_{bs}, respectively, and a single-scattering albedo, $(\tau_{ext} - \tau_{abs})/\tau_{ext}$, of 0.88 which compares reasonably well with that reported for biomass burning aerosols in previous studies (0.83 ± 0.11) [*Radke et al.*, 1991]. Recalling that $I = I_o e^{-\tau}$, where I_o and I are the radiation intensities entering and exiting the optical medium, we calculate that for this case, of all 500-nm light incident at 10 km, 45% was scattered and 9% was absorbed before reaching 1.5-km altitude; of the amount scattered over this height interval, about 2% was returned directly to space.

The above calculations were repeated upon all TRACE A profiles which covered a significant altitude range and for which RH and aerosol data were available. Results are shown in Table 3. The tabulated single-scattering albedo values are in general agreement with those of previous studies [e.g., *Penner et al.*, 1992] and range from 0.75 in dry, fine aerosol dominated air masses to 0.90 in cases where, as a result of high humidity, large particles were abundant. Note that the integrated parameters of Table 3 vary by about 2 orders of magnitude between the continental (flights 6, 7, and 10) and the oceanic (flights 16 and 17) soundings. The values exhibited for flight 8, profile 2 are perhaps the most representative of clean southern hemisphere background air. These data were recorded in Pacific source air which had passed over South America without entraining significant surface pollutants [*Gregory et al.*, this issue]. This profile yielded a column-integrated dry aerosol mass of 0.004 g m^{-2} and an optical extinction depth of 0.019. These values are significantly lower than found for other Table 3 soundings of comparable depth, with two exceptions: profiles 2 and 9 of flight 17. In these cases, although aerosol-enhanced layers were found at middle to high altitudes, a thick layer of relatively clean, subtropical South Atlantic source air was present at the lower levels. Other profiles

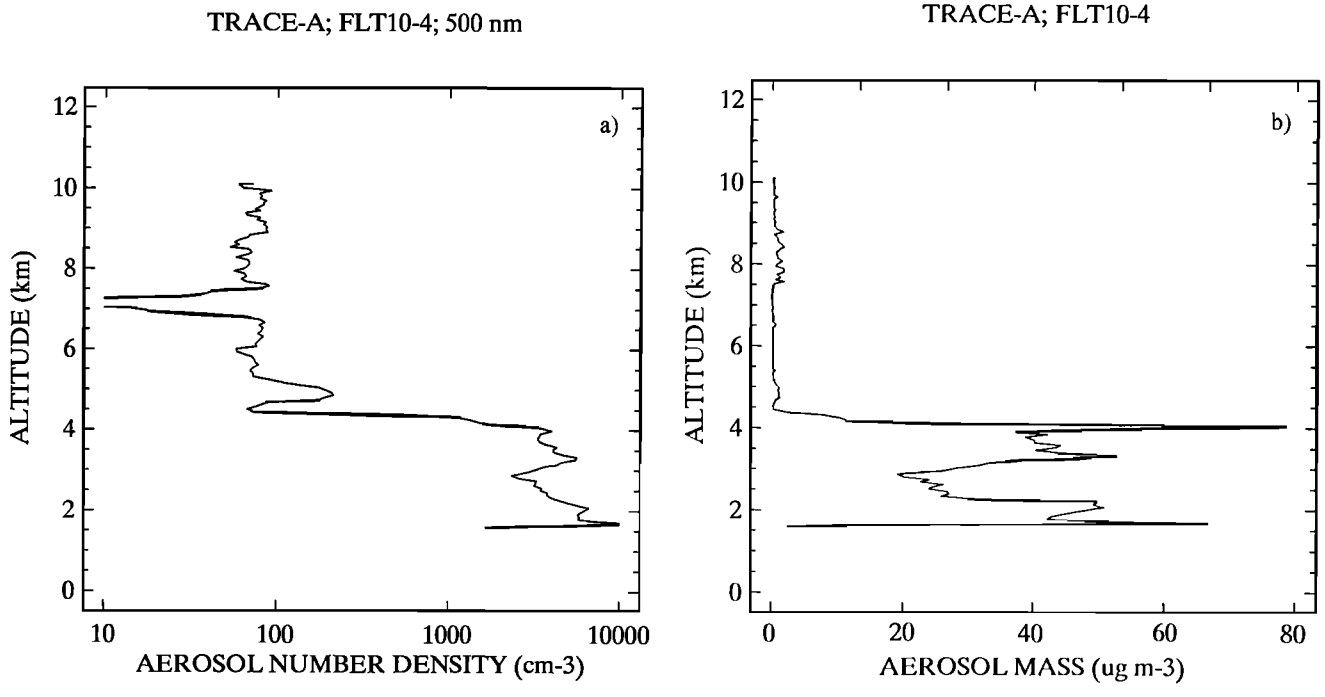

Figure 11. Vertical profiles of aerosol (a) number density, (b) mass, (c) extinction, (d) absorption, and (e) backscatter for data recorded through a smoke pall over an African savanna fire on flight 10. To illustrate the variation of aerosol concentration with height, the N and M profiles have not been corrected for temperature and pressure effects on air density. The aerosol mass are for the size range 0.1 to 3.0 μm and are corrected for RH effects. The optical parameters were calculated for 500-nm radiation making the assumptions described in the text.

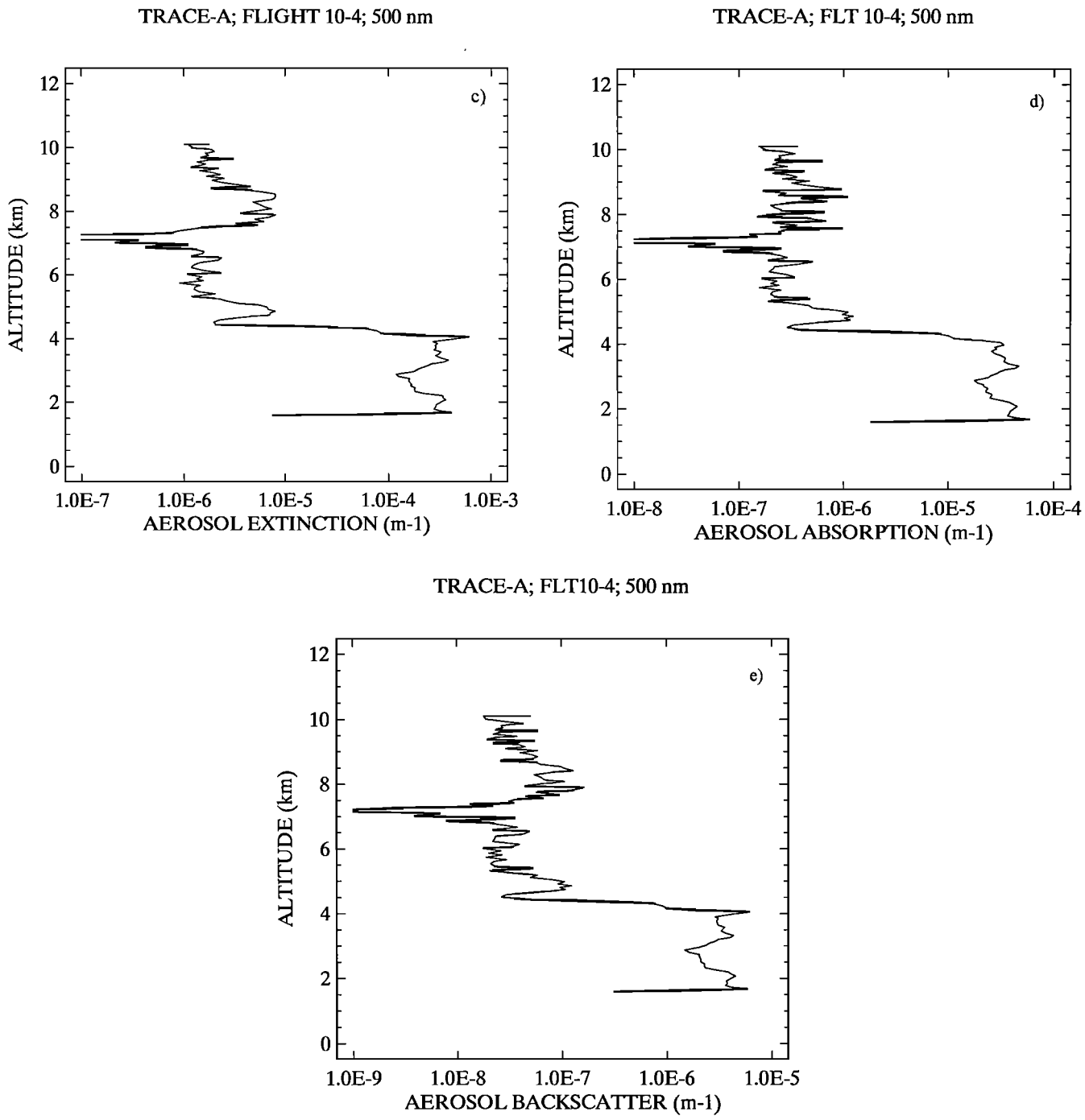

Figure 11. (continued)

from flight 17 show total mass and optical depths 2 to 3 times greater than the background case.

The maximum optical extinction and absorption depths of Table 3, 1.45 and 0.147, respectively, are for data acquired during flight 10, profile 8 through a smoke pall over an African savanna fire region. These values suggest a total loss of 77% of 500-nm radiation within the column, about 10% of which is absorbed and converted to heat energy. Although quite high, these values were, for several reasons, likely much lower than might be measured at a ground site with an upward looking radiometer. In addition to the fact that only aerosols in the 0.1- to 3.0-μm size range were measured and included in the calculation, the DC-8 was generally diverted around large, intense regions of smoke to prevent contaminating sample inlets and chemical instruments which were, for the most part, optimized for measuring trace species ordinarily present at substantially lower concentrations. The aircraft was also restricted to a minimum flight level of 300 m above the surface and higher in cases of reduced visibility. At these altitudes, the low-height vegetation fire plumes were substantially diluted with background air. Indeed, the average DC-8-measured CO mixing ratio within the mixed layer corresponding to flight 10, profile 8 was about 500 ppbv; values much greater than this are

Table 3. Integrated Optical Properties for TRACE A Vertical Profiles Calculated for 500-nm Radiation

Flight	Profile	Start Time, UT, s	End Time, UT, s	Latitude, °N	Longitude, °E	Altitude Maximum, km	Altitude Minimum, km	Integrated Dry Mass, g/m^2	Integrated Extinction	Integrated Absorption	Integrated Backscatter	Single-Scatter Albedo
5	2	56105	58915	-28.2	-43.8	9.5	0.3	0.027	0.207	0.026	0.0028	0.87
5	3	59225	59815	-27.3	-44.9	3.1	0.3	0.016	0.097	0.015	0.0016	0.85
5	5	67205	68275	-16.3	-48.4	9.3	1.2	0.058	0.480	0.053	0.0060	0.89
6	2	38405	39835	-8.9	-44.3	9.5	0.7	0.026	0.169	0.024	0.0023	0.86
6	3	40385	40555	-8.2	-44.7	1.8	0.9	0.005	0.029	0.005	0.0004	0.85
6	4	43205	43975	-9.3	-48.5	5.8	1.7	0.019	0.167	0.019	0.0021	0.89
6	6	49385	51175	-9.0	-48.8	11.3	0.8	0.055	0.464	0.055	0.0057	0.88
6	7	52085	53515	-9.0	-46.3	8.0	0.6	0.074	0.724	0.076	0.0079	0.89
6	8	54845	56215	-9.1	-44.3	7.2	0.9	0.023	0.159	0.022	0.0021	0.86
6	9	56825	57895	-10.9	-44.9	7.8	0.7	0.012	0.082	0.011	0.0012	0.86
7	2	53825	55735	-11.9	-42.9	11.2	0.7	0.031	0.221	0.030	0.0030	0.86
7	3	55745	56395	-12.0	-43.0	4.3	0.8	0.015	0.103	0.014	0.0015	0.86
7	6	65345	66475	-12.6	-44.8	6.6	0.8	0.015	0.095	0.014	0.0015	0.85
8	2	52445	53695	-27.1	-42.1	8.3	0.4	0.004	0.019	0.004	0.0003	0.81
8	3	54005	54475	-27.6	-42.5	3.1	0.3	0.001	0.004	0.001	0.0001	0.81
8	4	56045	56515	-30.1	-44.9	3.1	0.3	0.002	0.006	0.001	0.0001	0.80
8	5	56525	57835	-30.2	-44.9	8.3	0.3	0.010	0.039	0.008	0.0007	0.79
8	6	60485	61735	-34.1	-48.6	8.1	0.3	0.009	0.039	0.007	0.0007	0.82
8	9	68405	69715	-23.3	-43.7	8.2	0.2	0.038	0.386	0.038	0.0046	0.90
10	3	30305	31915	-21.7	28.2	4.0	1.2	0.009	0.096	0.009	0.0012	0.91
10	4	36905	38275	-11.1	29.4	10.1	1.6	0.083	0.711	0.084	0.0084	0.88
10	5	38285	38635	-10.8	29.6	3.1	1.5	0.002	0.007	0.002	0.0003	0.77
10	6	39245	40015	-10.1	30.0	7.2	3.1	0.045	0.446	0.046	0.0048	0.90
10	8	41345	42475	-10.0	30.5	8.6	1.7	0.142	1.454	0.147	0.0160	0.90
10	9	43385	44275	-11.2	29.5	6.4	1.5	0.067	0.467	0.066	0.0065	0.86
12	1	28815	30475	-24.8	28.0	10.1	1.7	0.030	0.130	0.025	0.0020	0.81
12	2	32705	33835	-18.9	27.2	10.1	3.1	0.003	0.014	0.003	0.0003	0.82
12	3	36065	36355	-19.2	24.6	4.6	3.1	0.003	0.015	0.003	0.0002	0.82
12	4	39005	39535	-19.3	18.3	7.7	4.6	0.004	0.036	0.004	0.0004	0.89
12	5	39665	40675	-19.0	17.9	7.7	1.5	0.032	0.307	0.031	0.0036	0.90
12	6	41105	42895	-19.2	17.4	5.2	1.5	0.013	0.091	0.012	0.0013	0.87
13	3	36845	38395	-5.8	8.7	11.3	0.3	0.039	0.203	0.030	0.0025	0.85
13	4	39065	39535	-7.3	9.0	3.7	0.3	0.014	0.091	0.013	0.0013	0.85
13	6	44045	44815	-17.8	9.0	7.1	0.3	0.027	0.127	0.023	0.0018	0.82
13	7	45845	47575	-20.0	9.2	6.0	0.3	0.014	0.033	0.008	0.0006	0.75
15	3	50225	50695	-9.1	2.5	7.7	3.7	0.003	0.015	0.003	0.0002	0.83
15	4	51545	52015	-11.0	2.5	3.7	0.3	0.009	0.056	0.009	0.0009	0.84
15	5	52505	54415	-12.1	2.4	3.7	0.3	0.015	0.054	0.011	0.0009	0.79
16	7	51785	53315	-8.4	-15.5	7.4	0.2	0.007	0.048	0.007	0.0007	0.86
17	2	38705	40255	-17.9	-20.0	10.7	0.3	0.008	0.013	0.003	0.0002	0.76
17	3	40865	41335	-16.7	-19.2	3.0	0.2	0.003	0.012	0.002	0.0002	0.81
17	6	51305	53035	0.4	-10.4	11.6	0.3	0.009	0.070	0.009	0.0010	0.88
17	7	53645	53995	-0.6	-10.7	2.5	0.3	0.008	0.039	0.005	0.0005	0.86
17	9	57605	58915	-7.5	-14.3	7.6	0.2	0.003	0.023	0.003	0.0003	0.88

Particle size distributions and masses were corrected for ambient relative humidity using procedures described within the text.

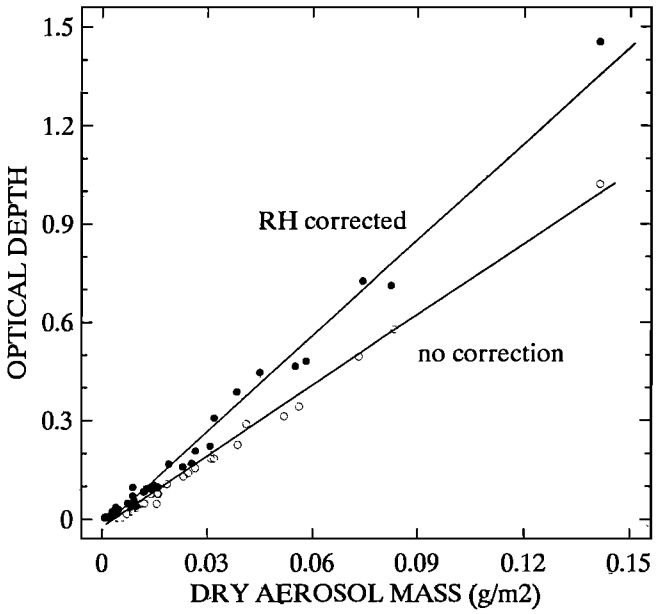

Figure 12. Plots of optical extinction depth at 500 nm versus dry aerosol mass for TRACE A vertical aerosol profiles before and after correction for aerosol growth due to RH effects.

common at surface sites within active burning regions [*Kirchhoff*, 1991]. Thus we suggest that the Table 3 source region values may significantly underestimate the local radiative impact of the fires.

The data of Table 3 can be used to calculate mass-dependent total optical cross sections for biomass burning aerosols. Figure 12 shows a plot of optical extinction depth calculated from both dry and humidity-corrected size distributions versus total dry aerosol loading. The slopes of these plots, 7.0 $m^2 g^{-1}$ and 9.6 $m^2 g^{-1}$, represent the mass extinction cross sections for the dry and humidity-corrected cases, respectively. For comparison, *Ferrare et al.* [1990] calculated a value for dry smoke of about 4.5 $m^2 g^{-1}$ and *Radke et al.* [1988] measured a value of 5 $m^2 g^{-1}$ in northern midlatitude forest fire plumes. This parameter is, of course, inversely dependent upon the aerosol mass density. If we had used a dry aerosol density of 1.5 g cm^{-3}, which is typical for sulfate-type aerosols, the above mass extinction cross sections would have been 4.7 and 6.4 $m^2 g^{-1}$, respectively. Values of total mass extinction, absorption, and backscatter cross sections for wavelengths of 350, 500, 600, and 1064 nm for dry and humidity-corrected biomass burning aerosol profiles are given in Table 4; these can be used in conjunction with Table 3 (and Table 5) integrated aerosol mass loadings to calculate optical depths at wavelengths other than the 500-nm shown. The cross section values increase with decreasing wavelengths due to the dominance of submicron particles in total aerosol mass loadings. The high extinction values at the shorter wavelengths suggest that smoke aerosols may greatly reduce the downward flux of photosynthetically active radiation and thus negatively impact the productivity of ecosystems within effected regions.

The average 500-nm optical characteristics of South Atlantic basin air masses are summarized in Table 5. These values were computed from averaged vertical profiles of aerosol number/size distributions and integrated from the surface to 12 km. The height-dependent aerosol size/number distributions were derived from all data recorded over the given region, including that from horizontal flight legs and vertical ascents/descents and regardless of whether sampling took place within clean background air or pollution-tainted continental plumes. The table is broken into categories of "fine" and "total" and "dry" and "wet" to illustrate the relative contribution of fine (0.1–0.9 μm) aerosols and the effect of humidity on calculated parameters. For these cases the fine aerosol comprised a mass fraction ranging from 47% (African outflow region) to 71% (Brazilian source region) of the total. This is less than the 80% seen in relatively fresh smoke plumes and may be caused by several factors, including a greater solubility (and hence wet removal rate) for the fine aerosols, a higher loading of coarse aerosols in the background air due to the dry conditions over the continents, and, particularly over the oceanic regions, input of sea-salt particles. Yet despite its reduced relative presence, the fine aerosols accounted for a large majority of the 500-nm optical extinction depth; their fractional contribution to this parameter ranged from about 77% to 90%. As noted above, the optical parameters are highly wavelength dependent and the coarse particles are expected to become of more relative importance to extinction of longer-wavelength radiation. For 500-nm light, the coarse mode particles do make a higher relative contribution to the optical absorption depth as the fine aerosol only account for about 60 to 80% of the total. We note, however, that the fractional absorption of the coarse aerosols may be overestimated in Table 5 due to our computationally simplifying assumption that the index of refraction remained constant across the entire aerosol size distribution. Although the coarse (or fine)

Table 4. Calculated Total Mass Optical Cross Sections for TRACE A Biomass Burning Aerosols for Various Wavelengths of Radiation Assuming a Wavelength-Independent Refractive Index for Dry Aerosols of 1.55–0.03*i*

	Wavelength							
	350 nm		500 nm		600 nm		1064 nm	
Parameter	dry	wet	dry	wet	dry	wet	dry	wet
Extinction	11.9	15.3	7.0	9.6	5.0	7.0	1.4	2.2
Absorption	1.55	1.54	1.02	1.02	0.80	0.81	0.36	0.37
Backscatter	0.127	0.166	0.089	0.108	0.080	0.101	0.048	0.060

Mass values are relative to an aerosol mass density of 1.0 g/cm^3. "Wet" values refer to calculations corrected for ambient relative humidity as described in the text.

Table 5. Calculated Optical Properties for 500-nm Radiation Obtained by Integrating Average Parameter Profiles Between the Surface and 12 km

TRACE A Geographic Region	Integrated Mass, g/m^2				Integrated Extinction				Integrated Absorption				Integrated Backscatter				Single-Scatter Albedo			
	Dry		Wet		Dry		Wet		Dry		Wet		Dry		Wet		Dry		Wet	
	Fine	Total	Fine	Total	Fine	Total	Fine	Total	Fine	Total	Fine	Total	Fine	Total	Fine	Total	Fine	Total	Fine	Total
South Atlantic	0.003	0.005	0.007	0.012	0.018	0.022	0.023	0.028	0.003	0.004	0.003	0.005	0.0003	0.0004	0.0004	0.0005	0.83	0.79	0.87	0.83
Brazilian source	0.029	0.041	0.065	0.087	0.184	0.205	0.226	0.255	0.029	0.036	0.029	0.038	0.0029	0.0034	0.0031	0.0037	0.84	0.82	0.87	0.85
African source	0.038	0.056	0.076	0.111	0.242	0.274	0.270	0.309	0.037	0.050	0.037	0.052	0.0038	0.0046	0.0040	0.0048	0.85	0.82	0.86	0.83
Brazilian outflow	0.017	0.028	0.042	0.068	0.110	0.129	0.143	0.170	0.017	0.024	0.017	0.026	0.0018	0.0024	0.0020	0.0026	0.84	0.81	0.88	0.85
African outflow	0.012	0.025	0.024	0.048	0.077	0.100	0.085	0.110	0.012	0.021	0.012	0.021	0.0012	0.0017	0.0013	0.0018	0.84	0.79	0.81	0.86

The "fine" columns represent calculations performed on 0.1- to 0.9-μm particles, whereas the "total" represents calculations which include 0.1- to 3.0-μm particles. "Dry" and "wet" refer to calculations for dry and humidity-corrected aerosol size distributions, respectively.

aerosol composition was not determined, it was likely different than that of the accumulation mode particles and, if predominantly composed of crustal components, was possibly much less absorbing than the 0.03 value for n_i used in our calculations would indicate.

The influence of ambient water vapor on aerosol optical extinction and backscatter depths was significant even though RH in the sampling regions seldom exceeded 60% and all data from within and near clouds were deleted from the data set under consideration. These results suggest that the direct radiative impact of the biomass burning aerosols could be greatly amplified in regions of high relative humidity. Indeed, using the RH corrections adopted in this paper and the mass cross-section information of Table 4, we calculate that the optical extinction depth of a parcel containing 0.1 g dry aerosol would increase from about 0.3 to 1.7 in going from 40 to 95% relative humidity. Such mixtures of aerosol loadings and humidities may be common over and within the persistent stratocumulus cloud decks of the eastern South Atlantic and could explain the large optical depths observed by remote sensors over that region during the tropical dry season [*Cahoon et al.*, 1995].

Table 5 results, when compared to background values (i.e., Table 3, flight 8, profile 2) suggest incident radiation was influenced by biomass burning aerosols at all locations within the South Atlantic basin during the TRACE A experiment. The average effect upon total extinction was relatively small in the clear-sky region of the middle South Atlantic, where optical depths were perhaps only 50% greater than background levels but significant over continental regions where this parameter was enhanced about an order of magnitude. The increased aerosol absorption depths perhaps had a greater impact upon regional radiation budgets because this parameter is, due to the low value of n_i for noncarbonaceous aerosols, ~0 in background air.

Direct Impact on Regional Radiation Budgets

The status of understanding the impact of biomass burning aerosols on the Earth's radiation budget as of 1994 is summarized by *Penner et al.* [1994]. Table 3 in that paper has values for a number of the key parameters required for calculating the radiative effects of biomass burning aerosols. While the values were thought to be representative of both temperate and tropical biomass burning, the numbers seem now to be more representative of temperate biomass burning than tropical mixed savanna/cerrado/forest burning. On the basis of recent results in the literature and the measurements and calculations reported here, we would like to propose a new set of values appropriate for Africa and Brazil. The parameters, *Penner et al.* [1994] values, and our values are presented in Table 6. The aerosol emission factor for the tropics is much lower in our estimate since the savannas and cerrados are characterized more by flaming fires than smoldering fires. The aerosol mass scattering and absorption efficiencies are based on the recent results from biomass burning in southern Africa [*Le Canut et al.*, 1996; *Scholes et al.*, 1996]. They are more representative of burning of savannas than are the results from temperate forests, although emissions from various ecoregions were included in making the determinations.

Using Tables 5 and 6 results, we can proceed to assess the impact of TRACE A observed aerosol loadings upon the regional radiation budget. In evaluating the effect of a layer of absorbing and reflecting aerosols above a reflecting surface, we start with the formalism for two reflective surfaces [*Charlson et al.*, 1991]. The equation for a nonabsorbing aerosol layer is

Table 6. Parameters for Biomass Burn Aerosols Relevant for the Earth's Radiation Budget From *Penner et al.* [1994] and Our Data

Parameter	Central Value*	Range*	Our Value	Reference
Emission factor (g/kg C in fuel)	32	18–52	12 ± 3*	*Le Canut et al.* [1996] *Scholes et al.* [1996]
Aerosol mass scattering efficiency† (m^2/g)	5	3.5–7	4.2	
Aerosol mass absorption efficiency† (m^2/g)	0.7	0.5–0.9	0.8	
Fractional increase in scattering due to hygroscopic growth	1.7	1.4–2.0		
Africa			1.14 ± 0.02	
Brazil			1.37 ± 0.14	
Wavelength to use for calculations	450–850 nm		600 nm	

*Assumes that 1 kg dry biomass = 0.45 kg C [*Crutzen and Andreae*, 1990].
†Dry aerosols.

$$R_{as}=R_a+T_a^2R_s/(1-R_aR_s) \quad (1)$$

where R_{as} is the reflectivity of the combined aerosol surface system; $R_{a(s)}$ is the reflectivity of the aerosol layer (surface); and T_a is the transmission of the aerosol layer as given by $T_a = 1 - R_a - A_a$, where A_a is absorption by the aerosol layer. We include aerosol layer absorption in the expression since biomass burning aerosols absorb, as opposed to sulfate aerosols, which do not [*Charlson et al.*, 1991]. Sample evaluations of (1) show that for low surface reflectivity compared with the aerosol reflectivity, there is cooling, as would be expected, but that for high surface reflectivity, there can be warming, since the aerosol layer absorbs some of the incident radiation.

We can solve (1) using the above data to estimate the change in radiation budgets for the TRACE A study area, an aerosol layer in central Africa. We first multiply the coefficients of Table 5 by a factor of 0.73 which is an estimate of the ratio of integrated average extinction over the entire solar spectrum to that calculated for 500 nm; this correction is necessary because, as pointed out by *Kiehl and Briegleb* [1993], use of the values appropriate for the solar maximum tends to overestimate the impact of biomass burning aerosols on the Earth's radiation budget. For surface albedos we use values for black earth or sea (0.06), green savanna (0.15), brown savanna (0.2), and stratus clouds (0.6) from *Budyko* [1956] and *Peixoto and Oort* [1992]. For the aerosol layer we assume that 30% of the scattered radiation is back into the hemisphere from which the incoming radiation came [*Penner et al.*, 1994]. We have then, $T_a^2 = 0.834$ for AS and 0.932 for AO, and $R_a = 0.0596$ for AS and 0.0195 for AO. For the solar insolation at the top of the atmosphere, we use 1365 W m^{-2}, an atmospheric transmission squared of 0.76 and a solar zenith angle of 15°. Thus the net 24-hour-averaged solar insolation reaching the Earth's surface in central Africa would be 500 W m^{-2}, ignoring the presence of clouds. The changes due to the aerosol layers over the various surfaces for the five major aerosol location classifications are given in Table 7, where negative values mean more radiation is reflected by the combined system. In Table 8 the changes in the atmospheric radiation budget are given, where absorption by the biomass burning aerosols as well as absorption by the atmosphere for the extra reflected radiation are combined. For the changes in atmospheric radiation balance we assumed that the atmospheric absorption was 10% of the change in Earth-surface insolation: for dry atmospheres, such as over Africa, water vapor absorption would be low; for moist atmospheres, such as over Brazil, absorption by water vapor for incoming solar radiation would reduce the amount of radiation that could be absorbed on the way back to space.

Thus we see that the average biomass burning plume reduces surface radiation by 10–25 W m^{-2} over land and sea but increases surface insolation over moderately thick clouds. The reduction over land and sea surfaces varies to 2.4 W m^{-2} for light aerosol loading. In addition, the aerosol layer absorbs some of the radiation that would have been absorbed and/or reflected by the Earth's surface, as does the entire atmosphere. The sum of the atmospheric and aerosol layer absorption always more than compensates for reduced surface absorption, except over very low albedo surfaces, due to the absorption by the aerosols.

Indirect Impact on Regional Radiation Budgets

In addition to the direct effects discussed above, we have also noted that changes in aerosol (CCN) abundance can indirectly

Table 7. Changes in Earth-Surface Insolation due to Biomass Burning Aerosols Based on Our Data

R_s	MSA		BS		AS		BO		AO	
	R_{as}	W/m^2	R_{as}	W/m^2	R_{as}	W/m^2	R_{as}	W/m^2	R_{as}	W/m^2
0.06	0.066	−3.0	0.106	-23.0	0.1103	26.5	0.093	−16.3	0.081	−10.5
0.15	0.156	−3.0	0.196	−23.0	0.203	26.5	0.183	−16.5	0.171	−10.5
0.2	0.206	−3.0	0.246	−23.0	0.253	26.5	0.233	−16.5	0.221	−10.5
0.4	0.406	−3.0	0.447	−23.5	0.454	−27.0	0.433	−16.5	0.421	−10.5
0.6	0.606	−3.0	0.647	−23.5	0.654	−27.0	0.633	−16.5	0.622	−11.0

Table 8. Changes in Earth-Atmosphere Radiation Budget Due to Biomass Burn Aerosols Based on Our Data

R_s	MSA, W/m^2	BS, W/m^2	AS, W/m^2	BO, W/m^2	AO, W/m^2
0.06	2.4	18.4	24.8	12.7	10.1
0.15	2.6	19.7	26.6	13.7	10.8
0.20	2.7	20.4	27.6	14.2	11.2
0.40	3.1	23.3	31.5	16.2	12.8
0.60	3.5	26.1	35.4	18.2	14.5

influence radiative budgets by altering the cloud microphysical parameters governing cloud albedo, persistence, water vapor content, and drizzle rate. Though the latter effects are difficult to quantify [*Albrecht*, 1989], *Twomey* [1991] has developed the following expressions to estimate the impact of CCN variations on cloud albedo:

$$d\tau/\tau = dN/3N \quad (2)$$

$$R_s = \tau/(13 + \tau) \quad (3)$$

where τ is cloud optical depth, N is the CCN number density, and R_s is the cloud reflectance as described above.

Pollution-related albedo changes may, in particular, have serious radiative consequences for the central/eastern South Atlantic region where large spatial regions (>10,000 km^2) are frequently covered by a low-level stratocumulus cloud deck. As shown in Plate 1, aerosol-enhanced, biomass burning plumes from Africa were often observed to overlie these clouds and the relatively rapid subsidence prevalent along the eastern and northern periphery of the subtropical oceanic high coupled with radiative cooling

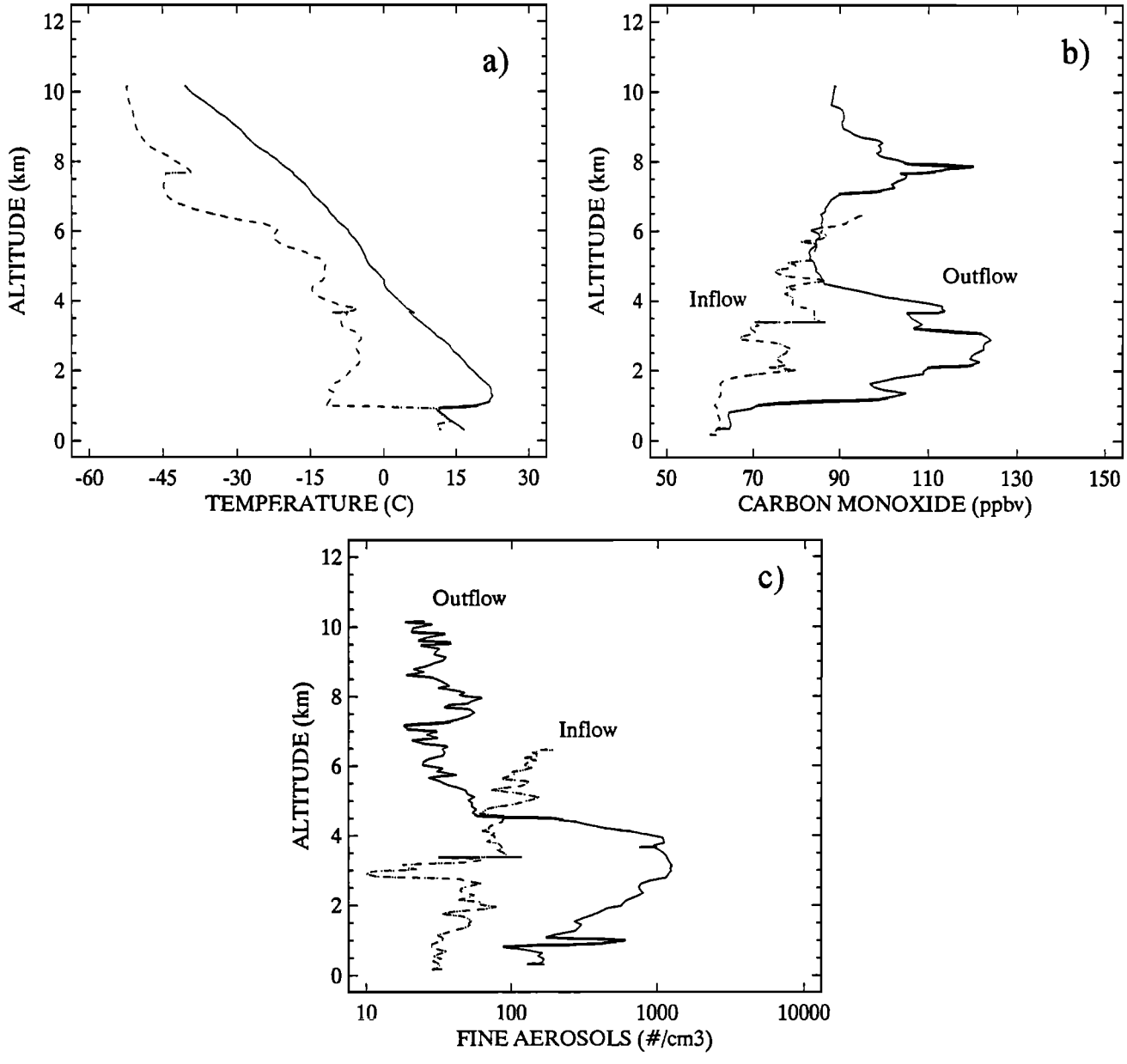

Figure 13. Profiles of (a) temperature and dew point, (b) CO, and (c) N recorded on flight 15 near 10°S, 3°E on flight 15 (meteorological profiles and "outflow" soundings) and near 35°S, 30°W on flight 11 ("inflow" profiles).

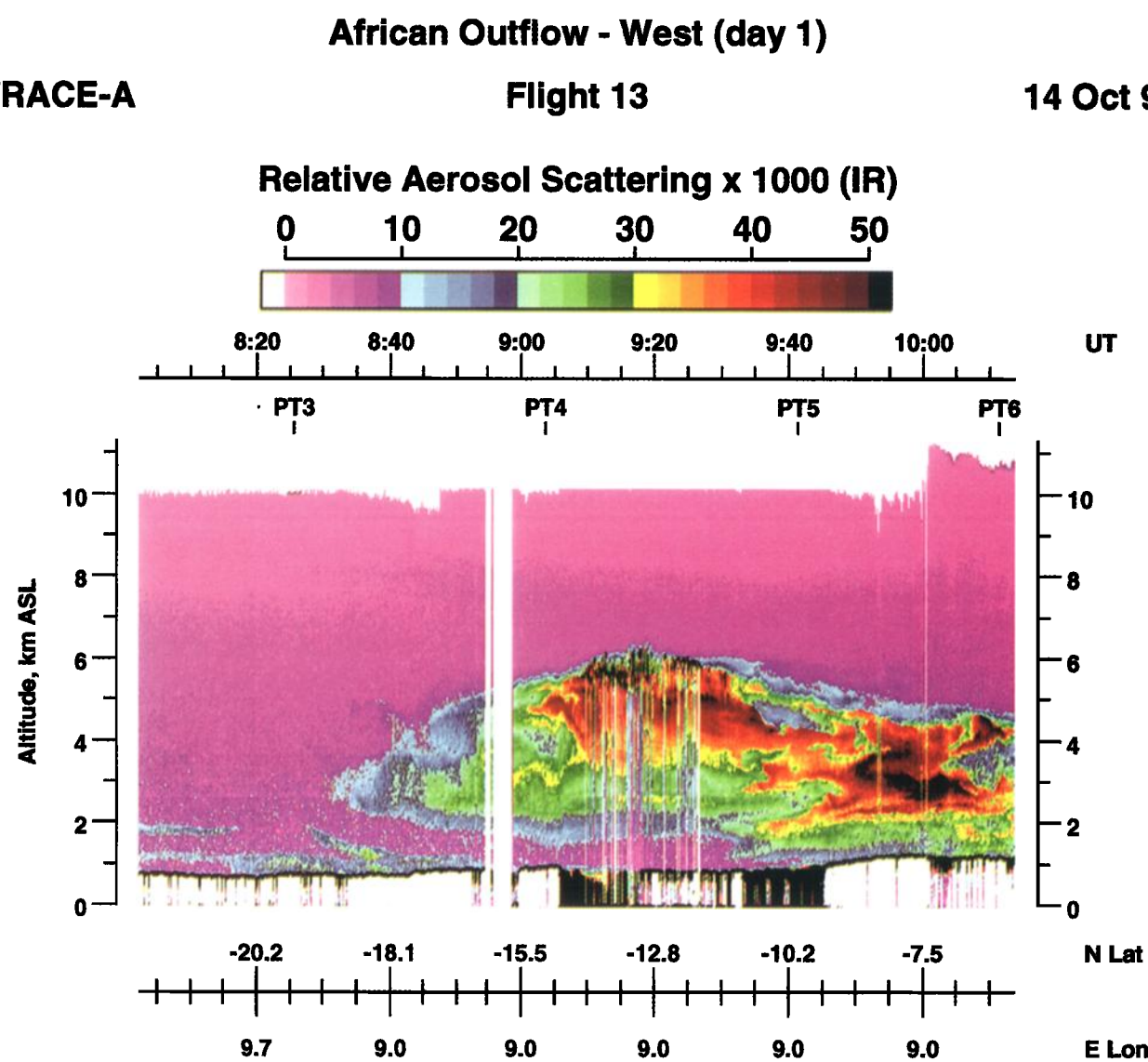

Plate 1. UV-DIAL cross section of aerosol backscattering recorded on flight 13 over the South Atlantic off the African coast showing an intense layer of aerosols residing just above a marine stratocumulus deck.

at the cloud tops generally led to downward mixing of these pollutants into the marine boundary layer [*Heikes et al.*, this issue].

The Figure 13 data provide a case study for evaluating the radiative impact of biomass aerosols on the stratus deck. These were recorded within, primarily, African continental outflow and inflow regimes on flight 15 near 10°S, 3°W over the stratocumulus-covered, eastern Atlantic and on flight 11 near 35°S, 31°W over a clear-sky region of the western Indian Ocean, respectively. The profiles (Figure 13a) indicate the Atlantic stratus deck was 300–500 m thick, topped out near 1 km altitude, and at the location of the soundings was, according to trajectory analyses, overridden by a dense layer of several-day-old African biomass burning pollution. Aerosol density within this layer reached ~1200 cm^{-3} near 3 km altitude and averaged 600 cm^{-3} in the km of air residing just above cloud top. Within the marine boundary layer (MBL), which trajectory analyses suggest was primarily influenced by subtropical South Atlantic source air, number densities averaged 150 cm^{-3}. The Figure 13b N profile recorded within relatively clean air suggests aerosol loadings would, in the absence of direct continental pollution, potentially be <100 cm^{-3} below 5 km altitude and around 30–50 cm^{-3} within the MBL. Thus assuming the ratio of CCN to N was the same for the clean and polluted cases, N = 50 and dN = 100 cm^{-3} within the cloud-forming MBL, and R_s = 0.6 [*Peixoto and Oort*, 1992], we calcu late the cloud reflectance increased by 0.11 as a result of biomass pollution. This, adopting the same assumptions as above, corresponds to a change of solar insolation at the surface of –42 W m^{-2}, which is 60–100% greater than the maximum calculated for the direct aerosol radiative impact over continental source regions.

Summary and Conclusion

The above presentation indicates that aerosol loadings over all regions of the tropical South Atlantic basin visited during TRACE A were significantly enhanced as a result of biomass burning occurring both in South America and in Africa. Results of simple calculations strongly suggest that these enhancements had a significant direct and indirect impact on regional radiation

budgets. We note, however, that TRACE A was conducted at a time when burning activity was greatly reduced in Brazil because of unusually wet conditions and Africa because of draught. Thus it is likely that the observed fine aerosol loadings may be significantly lower than seen during the peak of typical dry seasons over the South Atlantic basin. Thus it seems reasonable to anticipate that our results could significantly underestimate aerosol spatial distributions and impacts at the peak of fire activity in a typical burning season.

Clearly, additional, longer-term research is warranted to investigate the physical/chemical characteristics of these aerosols and their influence on incident radiation fields. Compositional, morphological, optical, and more extensive size distribution measurements of these aerosols as a function of fuel-type and fire conditions are particularly needed in order to reduce uncertainties in the mass and direct radiation budget calculations. A comprehensive investigation of biomass burning emission influence on cloud microphysical properties should also receive high priority in order to place constraints on the indirect impact of the aerosol on hydrologic cycles and surface albedo.

Acknowledgments. We wish to thank the DC-8 crew and support team for their assistance during the field deployment. We also thank J. M. Hoell Jr. and W. R. Cofer III (NASA Langley Research Center) and two anonymous reviewers for their useful reviews and suggestions during the preparation of this manuscript. This work was supported by the NASA Global Tropospheric Experiment Program.

References

Ackerman, T. P., and O. B. Toon, Absorption of visible radiation in atmosphere containing mixtures of absorbing and nonabsorbing particles, *Appl. Opt., 20*, 3661–3668, 1981.

Albrecht, B. A., Aerosols, cloud microphysics, and fractional cloudiness, *Science, 245*, 1227–1230, 1989.

Anderson, B. E., G. L. Gregory, J. D. W. Barrick, J. E. Collins, G. W. Sachse, C. H. Hudgins, J. D. Bradshaw, and S. T. Sandholm, Factors influencing dry season ozone distributions over the tropical South Atlantic, *J. Geophys. Res., 98*, 23,491–23,500, 1993a.

Anderson, B. E., G. L. Gregory, J. D. W. Barrick, J. E. Collins, G. W. Sachse, C. H. D. Bagwell, M. C. Shipham, J. D. Bradshaw, and S. T. Sandholm, The impact of U.S. continental outflow on ozone and aerosol distributions over the western Atlantic, *J. Geophys. Res., 98*, 23,477–23,489, 1993b.

Anderson, B. E., G. L. Gregory, J. E. Collins, G. W. Sachse, T. J. Conway, and G. P. Whiting, Airborne observations of the spatial and temporal variability of tropospheric carbon dioxide, *J Geophys. Res., 101*, 1985–1997, 1996.

Andreae, M. O., et al., Biomass-burning emissions and associated haze layers over Amazonia, *J. Geophys. Res., 93*, 1509–1527, 1988.

Andreae, M. O., A. Chapuis, B. Cros, J. Fontan, G. Helas, C. Justice, Y. J. Kaufman, A. Minga, and D. Nganga, Ozone and Aitken nuclei over equatorial Africa: Airborne observations during DECAFE 88, *J. Geophys. Res., 97*, 6137–6148, 1992.

Andreae, M. O., B. E. Anderson, D. R. Blake, J. D. Bradshaw, J. E. Collins, G. L. Gregory, G. W. Sachse, and M. C. Shipham, Influence of plumes from biomass burning on atmospheric chemistry over the equatorial and tropical South Atlantic during CITE 3, *J. Geophys. Res., 99*, 12,793–12,808, 1994.

Bachmeier, A. S., and H. E. Fuelberg, Meteorological overview of the Transport and Atmospheric Chemistry Near the Equator—Atlantic (TRACE A) experiment, *J. Geophys. Res.*, this issue.

Bingemer, H. G., M. O. Andreae, T. W. Andreae, P. Artaxo, G. Helas, D. J. Jacob, N. Mihalopoulos, and B. C. Nguyen, Sulfur gases and aerosols in and above the equatorial African rain forest, *J. Geophys. Res., 97*, 6207–6217, 1992.

Blake, D. R., et al., Biomass burning emission factors of selected trace gases source strength estimates of various NMHCs and halocarbons, *J. Geophys. Res.*, this issue.

Bohren, C. F., and D. R. Huffman, *Absorption and Scattering of Light by Small Particles*, 530 pp., John Wiley, New York, 1983.

Browell, E. V., Differential absorption lidar sensing of ozone, *Proc. IEEE, 77*, 419–432, 1989.

Browell, E. V., et al., Ozone and aerosol distributions and air mass characteristics over the South Atlantic basin during the burning season, *J. Geophys. Res.*, this issue.

Budyko, M. I., *The Heat Balance of the Earth's Surface*, St. Petersburg, Russia, 1956. (Translated from the Russian by U.S. Weather Bur., Washington, D. C., 1958.)

Cahoon, D. C., Jr., B. J. Stocks, J. S. Levine, W. R. Cofer III, and K. P. O'Neill, Seasonal distribution of African savanna fires, *Nature, 359*, 812–815, 1992.

Charlock, T. P., and W. D. Sellers, Aerosol, cloud reflectivity and climate, *J. Atmos. Sci., 37*, 1136–1137, 1980.

Charlson, R. J., J. E. Lovelock, M. O. Andreae, and S. G. Warren, Oceanic phytoplankton, atmospheric sulphur, cloud albedo and climate, *Nature, 326*, 655–661, 1987.

Charlson, R. J., J. Langner, H. Rodhe, C. B. Leovy, and S. G. Warren, Perturbation of the northern hemisphere radiative balance by backscattering from anthropogenic sulfate aerosols, *Tellus, 43AB*, 152–163, 1991.

Charlson, R. J., S. E. Schwartz, J. M. Hales, R. D. Cess, J. A. Coakley Jr., J. E. Hansen, and D. J. Hofmann, Climate forcing by anthropogenic aerosols, *Science, 255*, 423–430, 1992a.

Charlson, R. J., S. E. Schwartz, J. M. Hales, R. D. Cess, J. A. Coakley Jr., J. E. Hansen, and D. J. Hofmann, Aerosols and global warming, *Science, 256*, 598–599, 1992b.

Chatfield, R. B., J. A. Vastano, H. B. Singh, and G. Sachse, A general model of how fire emissions and chemistry produce African/Oceanic plumes (O_3, CO, PAN, Smoke) seen in TRACE A, *J. Geophys. Res.*, in press, 1996.

Chuang, C. C., J. E. Penner, and L. L. Edwards, Nucleation scavenging of smoke particles and simulated drop size distributions over large biomass fires, *J. Atmos. Sci., 49*, 1264–1275, 1992.

Coakley, J. A., Jr., R. D. Cess, and F. B. Yurevich, The effect of tropospheric aerosols on the Earth's radiation budget: A parameterization for climate models, *J. Atmos. Sci., 40*, 116–138, 1983.

Coakley, J. A., Jr., R. L. Bernstein, and P. A. Durkee, Effect of ship-stack effluents on cloud reflectivity, *Science, 237*, 1020–1022, 1987.

Crutzen, P. J., and M. O. Andreae, Biomass burning in the tropics: Impact on atmospheric chemistry and biogeochemical cycles, *Science, 250*, 1669–1678, 1990.

Dave, J. V., *Subroutines for Computing the Parameters of the Electromagnetic Radiation Scattered by a Sphere*, IBM order number 360D-17.4.002, 1968.

Fishman, J., Probing planetary pollution from space, *Environ. Sci. Technol., 25*, 613–620, 1991.

Fishman, J., C. E. Watson, J. C. Larsen, and J. A. Logan, The distribution of tropospheric ozone determined from satellite data, *J. Geophys. Res., 95*, 3599–3617, 1990.

Fishman, J., J. M. Hoell Jr., R. D. Bendura, V. W. J. H. Kirchhoff, and R. J. McNeal, NASA GTE TRACE A experiment (September-October 1992): Overview, *J. Geophys. Res.*, this issue.

Fitzgerald, J. W., Approximation formulas for the equilibrium size of an aerosol particle as a function of its dry size and composition and the ambient relative humidity, *J. Appl. Meteorol., 14*, 1044–1049, 1975.

Fuelberg, H. E., J. D. VanAusdall, E. V. Browell, and S. P. Longmore, Meteorological-conditions associated with vertical distributions of aerosols off the west coast of Africa, *J. Geophys. Res.*, this issue.

Gregory, G. L., H. E. Fuelberg, S. P. Longmore, B. E. Anderson, J. E. Collins, and D. R. Blake, Chemical characteristics of tropospheric air over the tropical South Atlantic Ocean: Relationship to trajectory history, *J. Geophys. Res.*, this issue.

Hagen, D. E., M. B. Trueblood, and D. R. White, Hydration properties of combustion aerosols, *Aerosol Sci. Technol., 10*, 63–69, 1989.

Hao, W. M., and M.-H. Liu, Spatial and temporal distribution of tropical biomass burning, *Global Biogeochem. Cycles, 8*, 495–503, 1994.

Heikes, B., M. Lee, D. Jacob, R. Talbot, J. Bradshaw, H. Singh, D. Blake, B. Anderson, H. Fuelberg, and A. M. Thompson, Ozone, hydroperoxides, oxides of nitrogen, and hydrocarbon budgets in the marine boundary layer over the South Atlantic, *J. Geophys. Res.*, this issue.

Jacob, D. J., et al., Origin of ozone and NO_x in the tropical troposhere: Photochemical analyis of aircraft observations over the South Atlantic basin, *J. Geophys. Res.*, this issue.

Kaufman, Y. J., A. Setzer, D. Ward, D. Tanre, B. N. Holben, P. Menzel, M. C. Pereira, and R. Rasmussen, Biomass Burning and Spaceborne Experiment in the Amazonas (BASE A), *J. Geophys. Res., 97*, 14,581–14,599, 1992.

Kiehl, J. T., and B. P. Briegleb, The relative roles of sulfate aerosols and greenhouse gases in climate forcing, *Science, 260*, 311–314, 1993.

Kim, Y. J., and J. F. Boatman, Size calibrations for the active scattering aerosol spectrometer probe (ASASP-100X), *Aerosol Sci. and Technol., 12*, 665–672, 1990.

Kirchhoff, V. W. J. H., Biomass burning in the Brazilian Amazon region: Measurements of CO and O_3, in *Global Biomass Burning: Atmospheric, Climatic, and Biospheric Implications*, edited by J. S. Levine, chap. 12, pp. 106–111, MIT Press, Cambridge, Mass., 1991.

Kirchhoff, V. W. J. H., J. R. Alves, F. R. da Silva, and J. Fishman, Observations of ozone concentrations in the Brazilian cerrado during the TRACE A field expedition, *J. Geophys. Res.*, this issue.

Le Canut, P., M. O. Andreae, G. W. Harris, F. G. Weinhold, and T. Zenker, Airborne studies of emissions from savanna fires in southern Africa, 1, Aerosol emissions measured with a laser-optical particle counter, *J. Geophys. Res.*, this issue, 1996.

Lenoble, J., The particulate matter from biomass burning: A tutorial and critical review of its radiative impact, in *Global Biomass Burning: Atmospheric, Climatic, and Biospheric Implications*, edited by J. S. Levine, chap. 46, pp. 381–386, MIT Press, Cambridge, Mass., 1991.

Li, J., and J. Mao, Properties of atmospheric aerosols inverted from optical remote sensing, *Atmos. Environ., 24A*, 2517–2522, 1990.

Peixoto, J. P., and A. H. Oort, *Physics of Climate*, Am. Inst. of Phys., New York, 1992.

Penner, J. E., S. J. Ghan, and J. J. Walton, The role of biomass burning in the budget and cycle of carbonaceous soot aerosols and their climate impact, in *Global Biomass Burning: Atmospheric, Climatic, and Biospheric Implications*, edited by J. S. Levine, chap. 47, pp. 387–393, MIT Press, Cambridge, Mass., 1991.

Penner, J. E., R. E. Dickinson, and C. A. O'Neill, Effects of aerosol from biomass burning on the global radiation budget, *Science, 256*, 1432–1433, 1992.

Penner, J. E., et al., Quantifying and minimizing uncertainty of climate forcing by anthropogenic aerosols, *Bull. Am. Meteorol. Soc., 75*, 375–400, 1994.

Pickering, K. E., et al., Convective transport of biomass burning emissions over Brazil during TRACE A, J. Geophys. Res., this issue.

Radke, L. F., J. L. Stith, D. A. Hegg, and P. V. Hobbs, Airborne studies of particulates and gases from forest fires, *J. Air Pollut. Control Assoc., 28*, 30–33, 1978.

Radke, L. F., J. H. Lyons, P. V. Hobbs, and R. E. Weiss, Smokes from the burning of aviation fuel and their self-lofting by solar heating, *J. Geophys. Res., 95*, 14,071–14,076, 1990a.

Radke, L. F., J. A. Coakley, and M. D. King, Direct and remote sensing observations of the effects of ships on clouds, *Science, 246*, 1146–1149, 1990b.

Radke, L. F., D. A. Hegg, P. V. Hobbs, J. D. Nance, J. H. Lyons, K. K. Laursen, R. E. Weiss, P. J. Riggan, and D. E. Ward, Particulate and trace gas emissions from large biomass fires in North America, in *Global Biomass Burning: Atmospheric, Climatic, and Biospheric Implications*, edited by J. S. Levine, chap. 28, pp. 209–224, MIT Press, Cambridge, Mass., 1991.

Scholes, R. J., D. Ward, and C. O. Justice, Emissions of trace gases and aerosol particles due to vegetation burning in southern hemisphere Africa, *J. Geophys. Res.*, in press, 1996.

Silver, D. M., N. deHaas, R. M. Fristrom, and M. J. Linevsky, Reactions of carbonaceous smoke particles with atmospheric ozone, *Aerosol Sci. Technol., 10*, 332–336, 1989.

Smyth, S. B., et al., Factors influencing the upper free tropospheric distribution of reactive nitrogen over the South Atlantic during the TRACE A experiment, *J. Geophys. Res.*, this issue.

Strapp, J. W., W. R. Leaitch, and P. S. K. Liu, Hydrated and dried aerosol-size-distribution measurements from the Particle Measuring Systems FSSP-300 probe and the deiced PCASP-100X probe, *J. Atmos. Ocean. Technol., 9*, 548–555, 1992.

Talbot, R. W., et al., Chemical characteristics of continental outflow over the tropical South Atlantic Ocean from Brazil and Africa, *J. Geophys. Res.*, this issue.

Twomey, S., *Atmospheric Aerosols*, 302 pp., Elsevier Sci., New York, 1977.

Twomey, S., Aerosols, clouds and radiation, *Atmos. Environ., 25A*, 2435–2442, 1991.

Twomey, S., M. Piepgrass, and T. L. Wolfe, An assessment of the impact of pollution on global cloud albedo, *Tellus, 36B*, 356–366, 1984.

Ward, D. E., Factors influencing the emissions of gases and particulate matter from biomass burning, in *Fire in the Tropical Biota: Ecosystem Processes and Global Challenges*, edited by J. G. Goldammer, pp. 418–436, Springer-Verlag, New York, 1990.

Ward, D. E., A. W. Setzer, Y. J. Kaufman, and R. A. Rasmussen, Characteristics of smoke emissions from biomass fires of the Amazon Region—BASE A experiment, in *Global Biomass Burning: Atmospheric, Climatic, and Biospheric Implications*, edited by J. S. Levine, chap. 48, pp. 394–402, MIT Press, Cambridge, Mass., 1991.

Ward, D. E., et al., Smoke and fire characteristics for cerrado and deforestation burns in Brazil: BASE B experiment, *J. Geophys. Res., 97*, 14,601–14,619, 1992.

Westphal, D. L., and O. B. Toon, Simulations of microphysical, radiative, and dynamical processes in a continental-scale forest fire smoke plume, *J. Geophys. Res., 96*, 22,379–22,400, 1991.

Winkler, P., The growth of atmospheric aerosol particles with relative humidity, *Phys. Scr., 37*, 223–230, 1988.

Wood, C. A., and R. Nelson, Astronaut observations of global biomass burning, in *Global Biomass Burning: Atmospheric, Climatic, and Biospheric Implications*, edited by J. S. Levine, chap. 3, pp. 29–40, MIT Press, Cambridge, Mass., 1991.

B. E. Anderson (corresponding author), E. V. Browell, W. B. Grant, and G. L. Gregroy, Atmospheric Sciences Division, NASA Langley Research Center, MS 483, Hampton, VA 23681.

D. R. Bagwell and C. H. Hudgins, Operations Support Division, NASA Langley Research Center, Hampton, VA 23681.

D. R. Blake and N. J. Blake, Chemistry Department, University of California-Irvine, CA 92717.

J. E. Collins, Jr., Science and Technology Corporation, Hampton, VA 23665.

G. W. Sachse, Aerospace Electronic Systems Division, NASA Langley Research Center, Hampton, VA 23681.

(Received June 19, 1995; revised January 22, 1996;
accepted February 1, 1996.)